Processive translocation of cohesive and non-cohesive cohesin *in vivo*

Running Title: Processive translocation of cohesin

Melinda S. Borrie and Marc R. Gartenberg[1,2]

Classification: Biological Sciences - Genetics

Department of Biochemistry and Molecular Biology
Robert Wood Johnson Medical School
Rutgers, The State University of New Jersey
Piscataway, NJ 08854

[1]Member of The Rutgers Cancer Institute of New Jersey, New Brunswick, NJ 08901
[2]Correspondence: marc.gartenberg@rutgers.edu

Keywords
cohesin, sister chromatid cohesion, transcription, Eco1, Wpl1

Abstract

Cohesin is a central architectural element of chromosomes that regulates numerous DNA-based events. The complex holds sister chromatids together until anaphase onset and organizes individual chromosomal DNAs into loops. Purified cohesin translocates along DNA in a diffusive fashion that can be propelled by transcribing RNA polymerase. The complex also extrudes DNA loops in a process that consumes ATP. In this study we examine processive genomic translocation of cohesin in vivo. To this end, obstacles of increasing size were tethered to DNA to act as roadblocks to complexes mobilized by transcription in yeast. The obstacles were built from a GFP-lacI core fused to one or more mCherries. A chimera with four mCherries blocked cohesin passage in late G1. During M phase, the threshold barrier depended on the state of cohesion: non-cohesive complexes were also blocked by four mCherries whereas cohesive complexes were blocked by as few as three mCherries. Furthermore, cohesive complexes that were stalled at obstacles, in turn, blocked the passage of non-cohesive complexes. That synthetic barriers alter cohesin redistribution demonstrates that the complex translocates processively on chromatin in vivo. The approach provides a relative measure of the maximum size of the DNA binding chamber(s) of cohesin. Together, this study reveals unexplored limitations to cohesin movement on chromosomes.

51 **Significance Statement**

52 Cohesin is an architectural protein that brings distant chromosomal DNA sites together. The
53 complex links sister chromatids cohesion but it also binds to single pieces of DNA in ways that
54 do not generate cohesion. One class of non-cohesive complexes organizes chromosomal DNA
55 into loops. All cohesin complexes move on DNA but the constraints on such movement are not
56 fully explored. Here, we use size-calibrated obstacles in yeast to interrogate cohesin and the
57 properties of its movement on DNA. We show that both cohesive and non-cohesive complexes
58 translocate processively on chromosomes. In addition, we show that cohesive and non-cohesive
59 complexes are blocked by obstacles of different size. Lastly, we show that stalled cohesive
60 complexes block passage of non-cohesive complexes.
61

Introduction

Cohesin is a central architectural element of chromosomes that functions by bringing distant DNA sites together (1). The protein complex was first characterized for its role in sister chromatid cohesion. Cohesin is now known to participate in most if not all fundamental chromosomal processes, including transcription, replication and repair. Recent work has shown that the complex also organizes chromosomes into large DNA loops that contribute to the segmentation of the genome into self-associating domains. Mis-regulation of cohesin has been identified as the cause of certain developmental diseases known collectively as cohesinopathies (2). Mutations in cohesin subunits have also been associated with human cancers.

The evolutionarily conserved core cohesin complex contains two SMC subunits (Smc1 and Smc3) and an α kleisin subunit Mcd1 (also known as Scc1/Rad21). The proteins assemble into a ring that can embrace DNA topologically, most notably when engaged in sister chromatid cohesion (3, 4). In yeast, the complex accumulates densely across tens of kilobases surrounding centromeres (5, 6). Along chromosome arms, the complex binds between convergently transcribed genes. Chromosome conformation capture (3C) techniques have shown that such sites participate both in sister chromatid cohesion and chromosomal loop formation in yeast (7-10). Cohesin performs these same architectural functions in higher eukaryotes (11-13).

Cohesin loading onto yeast chromosomes by NIPBL (Scc2 in yeast) begins each cell cycle in late G1. Initially, the interaction is dynamic. The complex cycles on and off DNA because loading is balanced by an unloading factor, WAPL (Wpl1 or Rad61 in yeast). During S phase, Eco1 (also known as Ctf7) halts cohesin loss by acetylating the Smc3 cohesin subunit, which antagonizes Wpl1 (14-18). Eco1 travels with the DNA replication fork, presumably to couple the stabilization of cohesive complexes directly with the creation of sister chromatids (19).

A second dynamic property of cohesin is the ability to redistribute on chromosomes. Cohesin accumulates at genomic sites that are often great distances from where the complex initially loads (20). Initially, RNA polymerase was seen as a central driver of repositioning because cohesin on dormant or weakly transcribed genes was relocated downstream by transcriptional induction (5, 6, 21). At least three observations suggested that cohesin relocates by processive

translocation: 1) at low temperature, gene induction moved the complex to intermediate positions between initial and final binding sites (22); 2) cohesin arriving at new sites following changes in transcription did not require the Scc2 loader for accumulation (22, 23); 3) cohesin mobilized by an ectopic polymerase in yeast redistributed to the end of the DNA travelled by the polymerase (24). Indeed, cohesin was shown to diffuse along DNA *in vitro*, and transcribing RNA polymerase was shown to bias the directionality of movement (24-26). More recent biochemical work showed that cohesin, in combination with NIPBL/Scc2, possesses an intrinsic motor activity that enables translocation of the complex along DNA in an ATP-dependent fashion (27, 28). Importantly, these studies showed that translocating cohesin can extrude DNA loops, an activity that is thought to form the large chromosomal loops that typify genomes (29-31). In support of the loop extrusion model, the size and distribution of chromosomal loops are altered by factors that influence the residence time of cohesin on chromatin (8, 9, 32-34).

We recently obtained evidence for processive cohesin translocation on chromosomal DNA in yeast using a system involving transcriptional induction of a cohesin bound gene (35). Upon induction of the gene, cohesion of the locus was lost. If, however, the locus was first converted to an extrachromosomal circle, cohesion persisted. The results are most readily explained by redistribution of topologically-bound cohesin complexes by processive translocation because such complexes cannot migrate off circularized DNA. In the present study, the properties of transcription-propelled complexes were further studied by measuring their ability to bypass synthetic obstacles of increasing molecular size. This work provides direct evidence that cohesin translocates processively on DNA *in vivo*. Moreover, the data reveal that the fate of encounters with barriers depends on the cohesive state of the complex: a barrier sufficient to trap cohesive complexes is not large enough to trap non-cohesive complexes.

Results

Nuclear membrane tethering of DNA blocks cohesin translocation

Our previous study found that DNA circularization, as well as downstream convergently oriented genes, prevented transcription-driven cohesion loss (35). As stated above, we inferred that circles trapped cohesin that was continuously mobile. Downstream convergent genes, on the other hand, were seen simply as barriers to cohesin passage. Intriguingly, DNA-bound lac repressors did not

124 block escape of cohesin (Figure 1A). We hypothesized that the bacterial protein (lacI fused to
125 GFP) was smaller than the chamber of the complex through which DNA passes. If topologically-
126 bound cohesin truly redistributes by translocation *in vivo*, then DNA-bound proteins of sufficient
127 size should block passage of the complex. To begin to explore this concept, we used a GFP-lacI
128 chimera linked to FFAT, a tetrapeptide motif that associates with the inner nuclear membrane
129 (36). When simultaneously tethered to DNA and the nuclear membrane, GFP-FFAT-lacI
130 represents an immobile obstacle of essentially infinite size (Figure 1A).
131
132 Translocation assays were performed at an engineered genomic locus (Figure 1B) that contains a
133 256 lac operator array downstream of *URA3*, a gene that can be induced 3-5 fold by withholding
134 uracil. Previous work showed that cohesive complexes associate with uninduced *URA3* until
135 transcriptional induction triggers their departure. Cohesin levels at the gene do not diminish,
136 however, because new complexes reload during the experimental interval ((35), see example in
137 figure S2). Here, chromatin immunoprecipitation coupled with quantitative real-time PCR
138 (ChIP-qPCR) was used to monitor arrival of cohesin at a downstream site immediately preceding
139 the lac operator array (hereafter referred to as the 5'lacO site). Immunoprecipitations were
140 performed with antibodies against a TAP epitope affixed to Mcd1.
141
142 *URA3* transcription was induced after cells were arrested in M phase by depletion of Cdc20.
143 When GFP-lacI was expressed, cohesin at 5'lacO was low both before and after *URA3* induction
144 (Figure 1C). The result is consistent with the inability of GFP-lacI to block translocating cohesin
145 complexes. Expression of GFP-FFAT-lacI, on the other hand, increased the level of cohesin at
146 5'lacO following transcription. This finding serves as a proof-of-principle that large immobile
147 objects block translocation of cohesin complexes in yeast. In *B. subtilis*, tethering a DNA-bound
148 repressor to the plasma membrane similarly blocked translocation of bacterial SMC proteins
149 (37).
150
151 <u>Large DNA-bound proteins block cohesin translocation</u>
152 To determine if large proteins could similarly block cohesin passage, a series of size-calibrated
153 obstacles was generated by fusing increasing numbers of mCherry to GFP-lacI (Figure 2A-C).
154 This red fluorescent protein is ideally suited as a size standard because it has a compact

155 monomeric structure unlike its tetrameric progenitor, DsRed (38-40). Like GFP-lacI, the
156 mCherry chimeras bind lacO arrays, albeit with reduced efficiency, as demonstrated by weaker
157 GFP foci and higher background nuclear fluorescence (Figure S1).
158
159 Accumulation of cohesin at 5'lacO was measured in M phase-arrested cells following three
160 different *URA3* induction protocols (Figure 2D). In the first, *URA3* was never induced.
161 Accordingly, cohesin levels at 5'lacO remained low and comparable to the cohesin-free control
162 site, which is represented by a dashed line in the figures. In the second protocol, *URA3* was
163 induced following imposition of an M phase arrest. In this case, accumulation of cohesin at
164 5'lacO depended on the identity of the GFP-lacI chimera expressed (Figure 2C). When GFP-lacI
165 was fused to one or two mCherries or none at all, cohesin levels did not rise above the baseline.
166 By contrast, when GFP-lacI was fused to three or four mCherries cohesin accumulated at 5'lacO.
167 A more thorough analysis of the cohesin distribution around the engineered locus is shown in
168 figure S2. In the three mCherry strain, the most dramatic changes in cohesin binding occurred
169 only between *URA3* and the lacO array, as expected for complexes travelling from the induced
170 gene into a downstream roadblock. No dramatic changes were found with GFP-lacI alone,
171 including at sites downstream of the array. This suggests that cohesin distributes throughout the
172 region in the absence of a single strong barrier. To be certain that an aberrant property of
173 mCherry was not responsible for 5'lacO accumulation, the experiment was repeated with a
174 chimera bearing three copies of monomeric yeGFP. Similar results were obtained (Figure S3).
175 These results indicate that DNA bound proteins of sufficient size block passage of translocating
176 cohesin complexes.
177
178 In the final experimental protocol, *URA3* was induced at the outset of asynchronous growth.
179 Previously we found that a downstream convergently-oriented gene could not block translocation
180 of cohesive complexes under these conditions. The basis for this phenomenon was not
181 understood (35). When *URA3* was induced from the outset here, most of the barrier chimeras
182 similarly failed to accumulate cohesin at 5'lacO. Some binding, however, was detected when
183 GFP-lacI was fused to four mCherries (Figure 2E). The data suggests that different sized barriers
184 act as obstacles under different conditions. Additional experiments elaborate on this concept
185 below.

186

187 Trapped cohesin complexes remain cohesive

188 To determine whether the complexes at 5'lacO hold sister chromatids together, we evaluated
189 cohesion of the chromosomal domain. In our strains, target sites for the R site-specific
190 recombinase flank the entire region (Figure 3A). Induction of the recombinase during an M
191 phase arrest generates a pair of DNA circles, one from each sister chromatid. Owing to the bound
192 GFP-lacI chimeras, a single dot of fluorescence appears if the DNA circles are cohesed whereas
193 a pair of dots appears if they are not (Figure S1). *URA3* transcription was induced according to
194 the three protocols described above and cohesion was evaluated at the end of the growth protocol
195 (Figure 3B). In the absence of induction, cohesion of DNA circles was observed in all strains due
196 to the presence of cohesive cohesin on *URA3* (Figure 3C; (35)). When transcription was induced
197 following M phase arrest, cohesion was greatly reduced in strains with chimeras bearing one or
198 two mCherries or none at all. This result indicates that these chimeras are too small to block
199 translocating cohesin. By contrast, cohesion persisted when transcription was induced in strains
200 expressing chimeras with three and four mCherries. Thus, consistent with the results in figure 2,
201 DNA-bound chimeras equal to or larger than three mCherries block passage of translocating
202 cohesive cohesin. We conclude that at least some of the trapped cohesin complexes detected by
203 ChIP-qPCR are engaged in sister chromatid cohesion.

204

205 When transcription was induced from the outset of cell growth, cohesion of the DNA circles was
206 abolished in all strains, irrespective of the chimera expressed. This result recapitulates the earlier
207 observation that convergent genes downstream of *URA3* also do not trap cohesive complexes
208 under identical induction conditions (35). These data suggest that the ability of an obstacle to
209 block passage of cohesin depends on the interplay between transcription and cell cycle stage.
210 Data supporting this view is presented below.

211

212 A larger barrier is required to block cohesin translocation in late G1 phase

213 The studies above examined translocation of cohesin on newly replicated chromatids in M
214 phase-arrested cells. To study translocation on unreplicated chromatin, cells were arrested in late
215 G1 by expressing a non-degradable allele of Sic1, a Cdk1 inhibitor that prevents S phase entry
216 (41). By definition, the chromatin-bound complexes at this stage of the cell cycle are not

217 cohesive. The steps of the growth protocol are depicted in figure 4A and validation of the growth
218 arrest is shown in figure S4. In this scenario, transcriptional induction caused accumulation of
219 cohesin at 5'lacO only in a strain expressing the four mCherry barrier. In strains expressing three
220 mCherries or GFP-lacI alone, cohesin accumulation matched the background levels of the
221 uninduced controls (Figure 4B). This data suggest that different size barriers are required to
222 block cohesin at different stages of the cell cycle. Apparently, something happens during S phase
223 that affects the how cohesin translocates past obstacles on DNA.
224
225 We hypothesized that the four mCherry threshold seen in figure 4B was related to the same
226 threshold seen during M phase arrest after induction from the outset of growth (Figure 2E). To
227 understand this line of reasoning, recall that cohesin binding resets after each anaphase passage
228 when separase activity subsides and Mcd1 synthesis resumes (42-44). If *URA3* is already
229 transcribing when cohesin binding resumes in late G1 then the ensuing translocation of the
230 complex would occur on an unreplicated chromosome, at least until S phase. Put simply,
231 translocation before DNA replication would bypass the three mCherry limitation normally seen
232 in M phase cells. To test this idea, *URA3* was induced from the outset of growth and barrier
233 activity of the obstacles was analyzed by ChIP-qPCR after cells were arrested in late G1. Figure
234 4C shows that cohesin accumulated at 5'lacO in cells that expressed a four mCherry obstacle but
235 not the three mCherry variant or GFP-lacI alone. These data indicate that when *URA3* is induced
236 from the outset of growth, transcription triggers translocation of cohesin before DNA replication,
237 leading to mobile complexes that pass obstacles the size of three mCherries but not four
238 mCherries.
239
240 <u>Translocation of complexes that arrive after DNA replication</u>
241 Cohesin loads continuously onto chromosomes from late G1 to anaphase (19, 35, 45).
242 Complexes that arrive after DNA replication are not cohesive, do not acquire S phase-dependent
243 acetylation and are subject to turnover by Wpl1 (46-50) To gain a more complete picture of
244 cohesin dynamics at *URA3*, transcription was induced while cells were arrested in late G1 and
245 then the cultures were released for growth into a subsequent M phase arrest. ChIP-qPCR at this
246 stage thus reports on those cohesin complexes that load and translocate to 5'lacO before S phase,
247 as well as those that load and translocate after S phase. Formally, this induction protocol also

248 records translocation of complexes that load during DNA replication of the gene, a time span that
249 is likely too short to affect the results significantly. The novel arrest-and-release procedure was
250 achieved by inducible clearance of AID-tagged, "non-degradable Sic1", using the auxin analog
251 1-naphthaleneacetic (Figure S4). The ChIP-qPCR data of figure 4D show that when *URA3*
252 transcription was induced, cohesin only accumulated at 5'lacO in the strain expressing the four
253 mCherry obstacle. That the barrier limit did not revert to three mCherries indicates that late
254 arriving, non-cohesive cohesin was not blocked by the smaller barrier.
255
256 To examine late arriving complexes exclusively, a TAP-tagged allele of Mcd1 was induced in M
257 phase arrested cells (Figure 5A). Subsequent induction of transcription caused accumulation of
258 TAP-tagged cohesin at the three and four mCherry obstacles (Figure 5B). On the surface, it
259 would appear that late arriving complexes cannot pass the smaller three mCherry barrier. In this
260 iteration of the experiment, however, untagged cohesive cohesin was created, having been
261 loaded earlier in the cell cycle. Accordingly, in this scenario cohesive cohesin stalled at three
262 mCherries might block passage of non-cohesive complexes. To test this notion directly, a second
263 iteration of the late-loading experiment was performed in which pre-existing cohesin was
264 removed during the M phase arrest by auxin-inducible degradation of endogenous Mcd1 (Figure
265 5A). Depletion of the AID-tagged protein was confirmed in figure S5. Figure 5C shows that the
266 late arriving TAP-tagged cohesin now bypassed the three mCherry obstacle and was instead
267 blocked by four mCherries (Figure 5C). The accumulation signal was weak but significant. Thus,
268 in the absence of cohesive cohesin, late-arriving, non-cohesive complexes stopped only at the
269 larger barrier to translocation. Importantly, the data show that stalled cohesive complexes block
270 the passage of non-cohesive complexes.
271
272 <u>Eco1 and Wpl1 modulate cohesin's encounters with barriers</u>
273 We next tested the influence of regulators of cohesin, Eco1 and Wpl1, on translocation of the
274 complex past synthetic obstacles. The proteins were depleted by auxin inducible degradation
275 during a G1 arrest, then cells were grown to the subsequent M phase arrest before inducing
276 *URA3* (Figures 6A). Clearance of the AID-tagged proteins is shown in figure S5A-C.
277 Transcriptional regulation of *URA3* was unchanged by the depletions (Figures S5D and S6B). In

278 these analyses, ChIP-qPCR data of transcribed and non-transcribed samples were always
279 compared to avoid impact that the mutants might have on absolute levels of cohesin binding.
280
281 When Eco1 was depleted the smallest obstacle, GFP-lacI alone, blocked cohesin translocation
282 (Figure 6B). This unexpected result was due specifically to loss of Eco1 because it did not occur
283 when DMSO was added instead of auxin (data not shown) or when Eco1 lacked the AID tag
284 (Figure 6C). The blockade was also dependent on the synthetic barrier: when Eco1 was depleted
285 from a strain lacking GFP-lacI accumulation of cohesin at the 5'lacO site was abolished (data not
286 shown). It appears that Eco1, presumably through Smc3 acetylation, facilitates translocation past
287 DNA-bound GFP-lacI.
288
289 To explore the phenomenon further, we examined cohesin translocation in a strain with an *smc1-*
290 *D1164E* allele. This mutation diminishes ATP-hydrolysis by cohesin, creating chromatin-bound
291 complexes that do not require Eco1 for protection against Wpl1 unloading (16, 51, 52).
292 Importantly, this mutation reduces Smc3 acetylation by Eco1 (52). In this strain, *URA3*
293 transcription during an M phase arrest also caused cohesin to accumulate at GFP-lacI alone
294 (Figure 6D). These results reinforce the notion that acetylation of Smc3 by Eco1 influences how
295 cohesin navigates the GFP-lacI array.
296
297 When Wpl1 was depleted, two notable changes occurred. First, depletion of the protein abolished
298 the three mCherry barrier, yielding a slight increase in accumulation at the four mCherry barrier
299 (Figure 6E). The small signal amplitude may be related to earlier observations that cohesin levels
300 are lower at enrichment sites in the absence of Wpl1 (9, 17, 18). These data suggest that cohesin
301 translocation is less restrained in the absence of Wpl1. The second notable change in figure 6E is
302 that accumulation of cohesin at the four mCherry chimera occurred even in the absence of *URA3*
303 induction. This feature is not unique to M phase-arrested cells. During late G1 arrest when
304 cohesin accumulates at the four mCherry chimera, loss of Wpl1 also eliminated the requirement
305 for *URA3* induction (Figure S6A). Misregulation of *URA3* in the absence of Wpl1 could explain
306 the results. However, *URA3* transcription was found to be normal (Figure S5D and S6B).
307 Instead, it seems that basal transcription of *URA3* is sufficient to cause cohesin accumulation at
308 synthetic obstacles in the absence of Wpl1. If cohesin binds less specifically in Wpl1 mutants

309 (53), and the residence time on DNA is longer (48), basal transcription of *URA3* might be
310 sufficient to mobilize mis-targeted complexes toward downstream synthetic barriers.
311
312 When Eco1 and Wpl1 were co-depleted, cohesin bypassed the three mCherry chimera yet the
313 complex was blocked efficiently by the larger four mCherry chimera (Figure 6F). Cohesin
314 accumulation did not require *URA3* induction, as seen before when depleting Wpl1 alone.
315 Interestingly, the paradoxical accumulation of cohesin at GFP-lacI in the absence of Eco1 was
316 abolished when both proteins were co-depleted. Apparently, the impact of Wpl1 depletion is
317 dominant when both proteins are absent. Perhaps with a longer DNA residence time conferred by
318 Wpl1 loss, cohesin eventually bypasses barriers with fewer than four mCherries.
319
320 Interpretation of the cohesin translocation results in the absence of Eco1 and Wpl1 requires
321 knowledge of the cohesive state of the complexes under study. Thus, we measured cohesion of
322 the chromosomal domain in the absence of the regulators. For simplicity, the experiments were
323 performed without transcriptional induction. Depletions were achieved during G1 arrest and then
324 cells were grown to an M phase arrest before DNA circles were excised. As expected, depletion
325 of Eco1 abolished cohesion (Figure 6G). Co-depletion of Eco1 and Wpl1 also yielded a severe
326 cohesion defect, as anticipated from earlier work (See (54), and references there in). Wpl1
327 depletion was previously shown to have an intermediate effect on chromosomal cohesion (17,
328 18, 54). Here, depletion of Wpl1 abolished cohesion of the locus under study. These data show
329 that the *URA3* gene is devoid of cohesive cohesin when Eco1 and or Wpl1 are depleted.
330 Therefore, complexes that translocate under these conditions due so on only one chromatid even
331 though both sisters are present.
332
333 **Discussion**
334 In this study we show that synthetic barriers of sufficient size cause ectopic accumulation of the
335 cohesin at synthetic roadblocks downstream of an inducible gene (Figure 2). That a DNA-bound
336 obstacle built entirely of non-yeast proteins blocks the passage of cohesin shows that the
337 complex translocates processively along DNA inside live cells. While our work was underway, a
338 study using nuclease-dead Cas9 as a barrier also showed that cohesin moves processively *in vivo*
339 (55). Our study goes further in three significant ways. First, we show that both cohesive and non-

340 cohesive complexes translocate processively on chromosomes. Second, we show that the two
341 types of complexes are blocked by barriers of different size (Figure 7A). Third, we show that
342 stalled cohesive complexes block passage of non-cohesive complexes (Figure 7B).
343
344 Cohesive cohesin has been shown to entrap both sister chromatids topologically within a single
345 complex (3, 4). Presumably, the cohesive cohesin that translocates in our studies is similarly
346 bound to DNA. Crosslinking studies have defined one large DNA chamber formed by the
347 interactions of core subunits (Smc1, Smc3 and Mcd1), as well as two smaller DNA chambers
348 partitioned from the larger chamber by the engaged heads of the Smc proteins (Figure 7C, (56)).
349 These and additional cryo-EM studies have mapped cohesin within the chambers of cohesin (57,
350 58). Synthetic obstacles of increasing size serve as a molecular ruler of the embrace of cohesin
351 through one or more of these chambers. Our work defines the upper size limit (measured in
352 mCherries) for cohesin's embrace of sister chromatids.
353
354 Non-cohesive cohesin can also bind single chromatids in a topological embrace but whether the
355 non-cohesive complexes in our studies are similarly bound is less clear (3, 4, 59). Biochemical
356 studies of cohesin translocation on single pieces of DNA have described active and passive
357 movements. In the active case, cohesin moved linearly along DNA and extruded DNA loops in
358 an ATP-dependent manner, the latter of which involved major conformational changes of the
359 complex (27, 28, 60). This type of movement required the continual action of NIPBL/Scc2, a
360 cofactor that stimulates the intrinsic cohesin ATPase activity (61). In congruence, loop extrusion
361 *in vivo*, as well as less defined modes of transport, have been linked to NIPBL/Scc2 (33, 62, 63).
362 For the following reasons, cohesin transport driven by NIPBL/Scc2 does not appear to involve
363 topological entrapment of DNA. To begin with, loop extrusion *in vitro* was observed with
364 crosslinked complexes that prevented DNA access to the central chamber (27). Moreover, a
365 recent biochemical study showed that loop extruding complexes bypassed roadblocks that
366 greatly exceeded the size of cohesin (64). Taken together, active movement of non-cohesive
367 cohesin does not appear to involve topological engagement nor require transcription as a motive
368 force.
369

370 In the passive movement case, topologically bound complexes were shown to travel in a
371 diffusional manner on DNA *in vitro* (24, 25). Such complexes gained directional mobility when
372 driven by transcribing RNA polymerase (24). Unlike loop extruding complexes, this type of
373 movement was blocked by DNA bound obstacles. Given that the cohesin complexes in our
374 studies were blocked by obstacles on DNA and that their movement required a transcriptional
375 trigger, it is reasonable to assume that they are of the topologically bound variety. Whether
376 NIPBL/Scc2 is recruited to complete cohesin transit all the way to a barrier, or whether non-
377 coding transcription beyond the *URA3* gene contributes is still under investigation.
378
379 The threshold size of an impassible barrier changed depending on when cohesin was loaded onto
380 chromosomes and when it translocated. Complexes loaded and transiting before S phase were
381 blocked by a four mCherry obstacle (Figure 4). Non-cohesive complexes loaded after S phase
382 were similarly blocked by a four mCherry barrier (Figure 5). Cohesive complexes, those which
383 were loaded before S phase but translocated after, were blocked instead by a three mCherry
384 barrier (Figures 2 and 3). Collectively, these observations suggest that the cohesive state of a
385 cohesin complex is the determinant of which mCherry barrier will block translocation. In this
386 scenario, the requirement of larger barriers to block non-cohesive complexes may simply reflect
387 the fact that these complexes entrap one less DNA duplex. In other words, non-cohesive
388 complexes translocate past smaller barriers because their DNA chambers are filled with less
389 DNA.
390
391 Both Eco1 and Wpl1 influence the size and distribution of chromosome loops in yeast, as do
392 their homologs in higher eukaryotes (8, 9, 27, 32, 33, 65, 66). Whereas Wpl1 restricts loop size
393 by limiting the residence time and location of cohesin on DNA, Eco1 is thought to restrict loop
394 size through a mechanism(s) independent of cohesion establishment. A simple hypothesis holds
395 that conditions which favor more extensive loop extrusion would also favor translocation past
396 smaller synthetic barriers. Indeed, simultaneous depletion of Eco1 and Wpl1 or just Wpl1 alone
397 increased the threshold size of a barrier in M phase cells from three mCherries to four mCherries
398 (Figure 6E and 6F). However, we showed that the locus under study was not cohesed in the
399 absence of Eco1 and Wpl1 (Figure 6G). Thus, a simpler explanation may prevail: the increase in

400 barrier size from three to four mCherries reflects the absence of cohesive complexes in these
401 mutants. This conclusion is entirely congruent with the cell cycle constraints described above.
402
403 Lastly, depletion of Eco1 alone yielded an entirely unexpected result: GFP-lacI alone was
404 sufficient to impede cohesin passage (Figures 6B). The observation was reinforced with an *smc1-*
405 *D1164E* mutant that hinders Smc3 acetylation by Eco1, as well as the intrinsic ATPase of
406 cohesin (Figure 6D). Recent studies have shown that acetylation by Eco1 plays a role in
407 anchoring the bases of cohesin-dependent loops (8, 65, 66). Whether the phenomenon is related
408 to this paradoxical result will require further investigation.
409
410 We have shown that cohesive cohesin at smaller barriers blocks passage of topologically-bound
411 non-cohesive complexes (Figure 5). A corollary to this conclusion is that sites of cohesin
412 accumulation in genome mapping studies may consist of both cohesive non-cohesive cohesin.
413 Recent mapping of cohesive cohesin in humans indicates that loop extrusion complexes do not
414 bypass cohesive complexes but instead help position them (13). It has also been argued that
415 stably bound cohesin complexes in yeast (possibly cohesive complexes) block passage of loop
416 extruders (9). This raises the possibility that stalled cohesive cohesin in our assays also blocks
417 passage of loop extruders. Maps of mammalian chromosomal loops often contain "stripes" that
418 are thought to be a signature of translocating loop extrusion complexes (67). Fine structure
419 mapping shows that stripes contain embedded dots, possibly from paused translocating
420 complexes (68). The synthetic barriers described here may mimic the natural impediments (e.g.
421 proteins bound at nucleosome depleted regions) that punctuate and terminate stripe patterns.
422 Whether stalled cohesive cohesin complexes or topologically bound non-cohesive complexes are
423 required for the punctuation of stripes remains to be determined.
424
425

426 **Materials and Methods**

427 *Yeast strains and plasmids*

428 Strains generated for this study were confirmed by PCR and/or DNA sequencing. Strains are
429 listed in Table S2 and primers are listed in Table S1. GFP-lacI with a linked SV40 NLS was
430 expressed from either a single or tandem integration of plasmid pGVH60, as noted in the strain
431 table. These integrants were modified by PCR-mediated gene tagging using multimeric repeats
432 of mCherry from plasmids pMAM12 and pMAM44 or three yeGFP(A206R)s from plasmid
433 pMAM88. Strains with tandem pGVH60 thus yielded simultaneous expression a GFP-lacI
434 chimera and GFP-lacI alone. Strains co-expressing GFP-lacI/GFP-lacI-mCherry chimeras,
435 however, produced identical results to strains expressing the mCherry chimeras alone (compare
436 figures 4C and S7). Integrating plasmid pXDA2-FFAT was assembled by *in vivo* recombination
437 from pAFS144-FFAT and pXRA2 (69). pXDL2-GAL1p-Sic1(4m)-AID*-9xmyc was similarly
438 assembled from pXRL2 (69), pRS306-GAL-Mt-4A-SIC1-HA-HIS6-Act (41) and pKan-AID*-
439 9myc (70). Integrating plasmid pXDnMX-GAL1p-Scc1(R180D,R268D)-TAP was assembled by
440 in vivo recombination from YIplac128-GAL1p-Scc1(R180D,R268D)-3xHA (LEU2), pXDnMX
441 (69), and a PCR fragment containing a TAP tag. Other genomic AID-tagged genes were
442 constructed by PCR tagging with the 3xmAID-5xflag module from pST1933 (NBRP ID:
443 BYP8880; (71)). OsTir1 was from integrated pTIR5 (*ADH1p-OsTIR1-CaADH1t,* Thomas Eng
444 thesis, U.C. Berkeley*)* or integrated pMSB27 (*ADH1p-OsTIR1*(yeast codon optimized)), which
445 was derived by *in vivo* recombination from pXRT1 (69) and pMK200 (NBRP ID: BYP7569).
446

447 *Cell growth and arrest*

448 To arrest cells in M phase for ChIP-qPCR, methionine was added (Cf = 2mM) to mid-log
449 cultures grown in SC-met to shut-off *MET3p-cdc20*. After 2.5 hours (roughly 80% of the cells
450 adopted a dumbbell shape), cells were washed twice with water and resuspended in SC media
451 lacking uracil to induce *URA3*. Two hours later the cultures were fixed for ChIP, according to
452 (35). To arrest cells in M phase for analysis of cohesion, cultures were grown in SC-met plus
453 dextrose for 6-8 hours and then diluted 200-400 fold into SC-met plus raffinose for overnight
454 growth. When cells reached mid-log the following morning, methionine was added. 150 minutes
455 later, cells were washed twice and resuspended in SC media lacking uracil. Two hours later,
456 galactose was added (Cf = 2%) to induce circularization by the R recombinase. Cells were fixed

457 with paraformaldehyde after two additional hours. To arrest cells for ChIP in late G1, dextrose
458 grown cultures were diluted 200-400 fold into SC-met plus raffinose for overnight growth. When
459 the cultures reached mid-log the following morning, alpha factor was added (Cf = 10 μM), and
460 90 minutes later galactose was added to induce expression of *GAL1p-SIC1(4m)-AID*-9xmyc*.
461 After one additional hour, cultures were washed twice with water and resuspended in SC-met
462 plus galactose and pronase E (Cf = 0.1 mg/ml) to release from pheromone arrest. One hour later,
463 the cells were washed twice and resuspended in galactose lacking both methionine and uracil.
464 Two hours later, the cultures were fixed for ChIP. For release from late G1 arrest, cells were
465 grown into the arrest as described above but with the following exceptions. After cells were
466 washed to remove alpha factor, they were resuspended in galactose media that lacked uracil but
467 contained methionine and pronase E. Two hours later, dextrose (Cf = 2%) was added to stop
468 expression of Sic1(4m)-AID*-9xmyc and 1-naphthaleneacetic acid (NAA, Cf = 100 μM) was
469 added to degrade the existing protein. Two hours later when cells accumulated in M phase,
470 cultures were fixed for ChIP. To express Mcd1-TAP exclusively in M phase, cells were arrested
471 in M by depletion of Cdc20, as described above. Two and half hours later, galactose was added
472 to induce expression of *GAL1p-MCD1(R180D,R268D)-TAP*. One hour later, NAA (or DMSO)
473 was added to degrade the existing Mcd1-3xmAID. Thirty minutes later, the cells were washed
474 twice with water and resuspended with the same media lacking uracil. Cells were fixed for ChIP
475 after an additional two hours. For depletion of the cohesin regulators, strains with the various
476 3xmAID alleles were treated with alpha factor for 90 minutes before adding NAA for 60
477 additional minutes. After release from alpha factor arrest, cells were resuspended in media
478 containing methionine for arrest in the subsequent M phase. 90 minutes later, cells were washed
479 twice before resuspending with media lacking uracil. Two hours later, cells were fixed for ChIP.
480 For cohesion assays involving protein depletions, cells were grown similarly except that cultures
481 were diluted into SC-met plus raffinose for overnight growth. In addition, galactose was added
482 once cells reached the M phase arrest and cells were fixed two hours later.
483
484 *Other techniques*
485 ChIP-qPCR, RT-qPCR and fluorescence microscopy were performed as described in (35). For
486 ChIP-qPCR, the mean and standard deviation of three or more biological replicates are
487 presented, unless specified otherwise. All values were normalized to an unlinked cohesin-bound

site (549.7 kb on Chr IV). Statistical significance was determined by pairwise Student's t tests relative to the induced 0x mCherry strain, unless specified otherwise. Immunoblots were probed with anti-GFP (G1544, Sigma), anti-myc (9E10, Roche), anti-mini-AID (M214-3, MBL), anti-Pgk1 (ab113687, Abcam) or anti-Rad23 (from the Madura laboratory), and secondary antibodies (W401B and W402B, Promega). ChIP was performed with anti-TAP and protein A Dynabeads (CAB1001 and 10001D, Invitrogen). A ChemiDoc instrument (BioRad) was used for gel imaging.

Acknowledgements

We thank the following individuals for reagents: Jason Brickner (pAFS144-FFAT), Michael Knop (pMAM12, pMAM44 and pMAM88), Kiran Madura (anti-Rad23), Adam Rudner (pTIR5), Benjamin Rowland (yeast BR423 *smc1-D1164E*) and Frank Uhlmann (YIplac128-GAL1p-Scc1(R180D,R268D)-3xHA (LEU2)). We thank Paul Kraycer for comments on the manuscript. This work was funded by United States Public Health Service Grant NIGMS 51402 (to M.R.G.) and a Busch Biomedical Grant from Rutgers University. The Flow Cytometry Core Facility of Robert Wood Johnson Medical School and The Rutgers Cancer Institute of New Jersey is supported by grants from the National Cancer Institute (Grant P30ES005022) and NIH (Grant S10OD026876).

Competing Interests

The authors declare that no competing interests exist.

511 **Figure legends**

512 **Figure 1** – Anchoring DNA to the inner nuclear membrane blocks cohesin translocation. **A)**
513 Schematic of transcription-triggered cohesin translocation and blockage by membrane
514 anchorage. Only one GFP-lacI is shown for clarity. NE = nuclear envelope. **B)** Schematic of the
515 locus used to test translocation. Binding of Mcd1 was evaluated at the 5'lacO site immediately
516 upstream of the lacO array. **C)** ChIP-qPCR of Mcd1-TAP. Strains MSB114 and MRG6947 were
517 arrested in M phase by Cdc20 depletion and then *URA3* transcription was induced. Values were
518 normalized to a cohesin bound site (see Materials and Methods). Measurements at a cohesin-free
519 site (534 kb on Chr IV) were averaged for all experiments of the figure panel and shown as a
520 dashed line. p values for pairwise Student's t tests are presented relative to benchmark sample
521 (designated with a dash). ns, not significant.

522

523 **Figure 2** – Synthetic barriers of sufficient size block cohesin translocation. **A**) Schematic of
524 transcription-triggered cohesin translocation and blockage by GFP-lacI chimeras. **B**)
525 Organization of the GFP-lacI chimeras with mCherries. **C**) Immunoblot of GFP-lacI chimeras.
526 Strains expressing MSB174, MSB179, MSB180, MSB181 and MRG7102 were used. The lower
527 molecular weight bands marked with * likely represent partial proteolytic cleavage of mCherry
528 (72). **D**) Experimental flow chart. Transcription was either induced from the outset of growth,
529 after M phase arrest or not at all. **E**) ChIP-qPCR of Mcd1-TAP. Cohesin binding at the 5'lacO
530 site was evaluated in strains MSB114, MRG6810, MRG6812, MSB165.1 and MRG7060.

531

532 **Figure 3** – Synthetic barriers of sufficient size block translocation of cohesive cohesin. **A**) An
533 assay for cohesion at a specific chromosomal location. The GFP-tagged region of interest is
534 converted to extrachromosomal circles by site specific recombination. Half-filled boxes
535 represent target sites for the inducible R recombinase. **B)** Experimental flow chart. **C**) Cohesion
536 analysis of extrachromosomal circles. Strains MSB35.2, MRG6806, MRG6808, MSB167 and
537 MRG7060 were used. p values for pairwise $\chi 2$ tests are presented relative to a benchmark
538 condition for each strain (designated with a dash). Error bars represent the standard error of
539 proportion. n = the number of cells examined.

540

541 **Figure 4** – Synthetic barriers to cohesin translocation before and after S phase. **A**) Experimental
542 flow chart. **B**) Barriers to translocation in late G1-arrested cells. ChIP-qPCR of Mcd1-TAP was
543 performed in strains MRG7027, MRG7026 and MRG7059 that were arrested by expression of
544 non-degradable Sic1. *URA3* transcription was induced after cell cycle arrest. **C**) Same as **B**
545 except transcription was induced from the outset of growth. Two trials were performed for each
546 strain. **D**) Barriers to translocation in cells progressing from G1 to M phase. Details of the cell
547 cycle arrest, release and re-arrest are described in Materials and Methods. Strains MRG7033,
548 MRG7032 and MRG7282 were used.
549
550 **Figure 5** – Translocation of cohesin complexes loaded in M phase. **A)** Experimental flow chart.
551 **B)** ChIP-qPCR of Mcd1-TAP**.** Strains MRG6989, MRG7294, and MRG7292 were used. The
552 Mcd1-TAP allele bears separase cleavage site mutations (R180D,R268D) that should not affect
553 the experimental outcome. The baseline levels of the Mcd1-TAP signal were higher in this
554 experiment relative to figures 2 and 4, likely owing to robust Mcd1 expression from the *GAL1*
555 promoter (45). Nevertheless, the relative levels were internally consistent with the previous
556 figures. **C)** ChIP-qPCR of Mcd1-TAP after depletion of endogenous Mcd1. Strains MRG7317.1,
557 MRG7319.1 and MRG7318.1 were used. See Materials and Methods for timing of each
558 experimental step. Cohesin did not accumulate at the three mCherry obstacle, unlike non-
559 cohesive complexes in figure 5B and cohesive complexes in figures 2E and 3C.
560
561 **Figure 6** – The impact of cohesin regulators on translocation past synthetic barriers. **A**)
562 Experimental flow chart. **B)** Translocation in the absence of Eco1. Eco1-3xmAID was depleted
563 by the addition of 100 μM NAA to strains MRG7301.1, MRG7300.1, MRG7302.1, as described
564 in Materials and Methods and graphically in panel A. p values for pairwise Student's t-tests are
565 presented for the transcriptional induction of each strain. **C)** Translocation in strains with Eco1.
566 Strains MRG7269.1, MRG7270.1 and MRG7275.1 express OsTir1 but lack AID-tagged genes.
567 **D)** The impact of *smc1-D1164E* on translocation past barriers. Strains MRG7151, MRG7146 and
568 MRG7159 were arrested in M phase before transcription was induced, as in figure 2. **E)**
569 Translocation in the absence of Wpl1. Wpl1 was depleted from strains MRG7327.1,
570 MRG7329.1, MRG7324.1. **F**) Translocation in the absence of Eco1 and Wpl1. Strains
571 MRG7332.1, MRG7356.1 and MRG7353.1 with 3xmAID alleles of *eco1* and *wpl1* were used.

572 **G)** Cohesion of the *URA3* locus in the absence of Eco1 and Wpl1. 3xmAID alleles were depleted
573 during G1 arrest before release into M phase arrest when DNA circles were excised. Strains
574 MSB203, MSB204, MSB205 and MSB206 were used.
575
576 **Figure 7 –** Processive translocation of cohesin *in vivo*. **A)** Cohesive cohesin cannot translocate
577 past a barrier larger than three mCherries during M phase. Non-cohesive complexes translocating
578 on single DNA (in late G1 or M phase) cannot translocate past a barrier larger than four
579 mCherries. That cohesin is mobilized by transcription and then arrests at obstacles suggests that
580 the complexes under study are bound topologically (see main text). **B)** Non-cohesive cohesin is
581 blocked by cohesive cohesin that has stalled at a 3xmCherry barrier. **C)** The chambers of
582 cohesin. The large topological compartment created by interactions of Smc3 and Smc1 with
583 Mcd1 is bisected into two smaller chambers by engagement of the Smc3 and Smc1 heads (filled
584 circles, (56)). The chamber(s) used during translocation have not yet been defined.
585
586 **Figure S1** – Representative images of cells expressing GFP-lacI chimeras. **A)** Strains MSB35.2,
587 MSB167 and MRG7060 were photographed after M phase arrest. Fluorescent protein chimeras
588 accumulated in the nucleus owing to a C-terminal SV40 NLS. Binding of GFP-lacI alone to the
589 lacO array yielded green foci with little background fluorescence. When chromatids separated,
590 two dots were seen (yellow arrows). Fusion of mCherries to GFP-lacI increased background
591 nuclear fluorescence, suggesting that the C-terminal addition to lacI interferes with chimera
592 binding. Nevertheless, sufficient binding occurred to yield discrete, albeit less intense foci. **B)** In
593 the absence of a lacO array (strains MRG7372, MRG7373 and MRG7374), no foci were seen,
594 indicating that GFP-lacI-mCherry chimeras do not intrinsically aggregate.
595
596 **Figure S2** – Cohesin distribution in strains expressing GFP-lacI-3xmCherry or GFP-lacI. **A)** A
597 map of the chromosome IIIR telomeric region bearing the engineered locus. Sites that were
598 analyzed are designated with lines and labels underneath the map. Drawn to scale. **B)** ChIP-
599 qPCR of Mcd1-TAP. Strains MSB165.1 and MSB114 were used. Transcription was induced
600 after M phase arrest.
601

602 **Figure S3** – A barrier consisting of GFP-lacI plus three copies of yeGFP. Strains MSB165.1 and
603 MRG7320 were used. Each of the three yeGFP multimers carries the A206R mutation that
604 abolishes weak dimerization of GFP (73). Cultures were grown as described in figure 2. Three
605 yeGFP(A206R) yielded the same result as three mCherries, indicating that residual
606 multimerization of mCherry or some other mCherry artifact was not responsible for barrier
607 activity. Two additional observations disfavor the notion that an aberrant property of mCherry is
608 responsible for barrier activity: 1) different sized obstacles are required at different stages of the
609 cell cycle (compare figures 2 and 4); 2) the timing of transcription determines the size of an
610 effective obstacle (figures 2 and 3). Loci with notably high changes in cohesin accumulation are
611 shown in red.
612
613 **Figure S4** – Stepwise cell cycle arrests using controlled expression of "non-degradable" Sic1.
614 **A**) Cell viability following induction and clearance of Sic1(4m)-AID*-9xmyc. Strains bearing a
615 *GAL1p-SIC1(4m)-AID*-9xmyc* allele (MRG7027 and MRG7033) were spotted in 10-fold serial
616 dilutions on the indicated plates. Galactose-induced lethality due to Sic1(4m)-9xmyc-AID*
617 expression was over-ridden by 100 μM 1-naphthaleneacetic acid (NAA), which triggers
618 degradation of the AID* chimera by OsTir1 in strain MRG7033. Methionine was omitted from
619 all plates for *MET3p-cdc20* expression. **B**) Validation of Sic1(4m) protein expression levels. The
620 same strains were grown according to the arrest and release protocol described in the Materials
621 and Methods. Lanes 1 and 5 = asynchronous growth in dextrose; lanes 2 and 6 = initial late G1
622 arrest in galactose media, one hour after removing alpha factor; lanes 3 and 7 = extended arrest at
623 late G1 in galactose media, three hours after removing alpha factor; lanes 4 and 8 = two hours
624 after adding NAA. Note that the myc-labelled Sic1(4m)-AID* band was cleared in lane 8
625 allowing this strain to advance to an M phase arrest. **C**) Validation of late G1 arrest by flow
626 cytometry. Strain MRG7027 was grown into a permanent late G1 arrest as described in Materials
627 and Methods, and used in figure 4B. DNA content was assessed in asynchronous culture, after
628 late G1 arrest and then after subsequent *URA3* induction. **D**) Validation of sequential cell cycle
629 arrests. Top row of panels - Dot plots of flow cytometry data (peak fluorescence vs fluorescence
630 intensity). Strain MRG7033 was used. Cells with clear 1N and 2N DNA content are shown in
631 navy blue and green, respectively. After a prolonged time in late G1 arrest, a large fraction of
632 cells (red) fell outside the gated area due to an elongated bud morphology (due to Sic1-

633 suppressed Cdk activity, (74)) that adversely affects peak fluorescence. Nevertheless, the data
634 show that cells shown in red shifted from 1N to 2N DNA content during progression from the
635 late G1 to M arrests. Bottom rows of panels - Direct visualization of cells and cell nuclei. The
636 percentage of cells that met the specified morphological criteria of each cell cycle arrest are
637 listed below the images. DNA was stained with Hoechst dye after ethanol fixation. n = number
638 of cells examined.
639
640 **Figure S5** – Depletion of Mcd1 and cohesin regulators. **A)** Cell viability following depletion of
641 Mcd1, Eco1 and Wpl1. Strains MRG7312.1, MRG7317, MRG7270.1, MRG7301.1,
642 MRG7327.1, MRG7332.1 and MRG7355.1 bearing the indicated *3xmAID* alleles and *OsTIR1*
643 were spotted in 10-fold serial dilutions on selective plates containing or lacking 100 μM NAA.
644 Depletion of Mcd1 or Eco1 caused loss of viability. Co-depletion of Eco1 and Wpl1 restored
645 viability. Similar results were obtained whether Wpl1 was depleted or the *WPL1* gene was
646 deleted, indicating that depletion phenocopied the null mutation. **B)** Camptothecin sensitivity
647 following Wpl1 depletion. Strains MRG7269.1, MRG7329 (isolate 1), MRG7329 (isolate 2) and
648 MRG6830.1 were spotted on SC-met containing or lacking 20 μg/ml camptothecin (CPT) and
649 100 μM NAA in 5-fold serial dilutions. Strains lacking Wpl1 were sensitive to the DNA
650 damaging agent (See (53) and references therein). The middle panel shows that tagging with
651 3xmAID slightly diminished the function of Wpl1. The right panel shows that depletion of the
652 protein with NAA phenocopied the null mutation. **C)** Depletion of 3xmAID-tagged proteins.
653 Strains MRG7317, MRG7301.1, MRG7327.1, and MRG7332.1 were used. Cells were grown to
654 mid-log in SC-met and treated with either 100 μM NAA or DMSO for 10 minutes for Mcd1
655 depletion and 60 minutes for the others. The tagged proteins were immunoblotted with an
656 antibody to mAID. **D)** RT-qPCR analysis of *URA3* mRNA following depletion of Eco1 and
657 Wpl1. Strains MRG7270.1, MRG7301.1, MRG7327.1, and MRG7332.1 were grown according
658 to the protocol described in figure 5A. Transcript levels were measured relative to *ACT1* mRNA
659 and normalized to a single trial of the uninduced wt control. The data show that loss of Wpl1 and
660 or Eco1 did not perturb normal *URA3* induction.
661
662 **Figure S6** – A synthetic barrier to cohesin translocation in late G1-arrested *wpl1Δ* cells. **A)**
663 ChIP-qPCR of Mcd1-TAP. Strains MRG7235.1, MRG7232.1 and MRG7238.1 were grown

664 according to the protocol described in figure 4A. Loss of Wpl1 caused accumulation of cohesin
665 at the four mCherry barrier without *URA3* transcriptional induction. **B)** RT-qPCR analysis of
666 *URA3* mRNA levels. Strains MRG7027 and MRG7235.1 were grown asynchronously before
667 RNA extracts were prepared. Values normalized as in figure S4. Loss of Wpl1 did not alter the
668 basal level of *URA3* transcription or the ability to induce the gene.
669
670 **Figure S7** – Barrier activity in strains expressing homogeneous GFP-lacI-mCherry chimeras.
671 *URA3* was induced in strains MRG7115 and MRG7122 after arrest in late G1 by Sic1(4m)-
672 AID*-9xmyc. Binding of cohesin at 5'lacO was analyzed by ChIP-qPCR of Mcd1-TAP. Barrier
673 function required four mCherries, similar to the results found with strains co-expressing the
674 mCherry chimeras along with GFP-lacI alone (Figure 4).

675 **References**

676 1. Davidson IF & Peters J-M (2021) Genome folding through loop extrusion by SMC
677 complexes. *Nat Rev Mol Cell Biol* 22:445-464.
678 2. Remeseiro S, Cuadrado A, & Losada A (2013) Cohesin in development and disease.
679 *Development* 140(18):3715-3718.
680 3. Haering CH, Farcas AM, Arumugam P, Metson J, & Nasmyth K (2008) The cohesin ring
681 concatenates sister DNA molecules. *Nature* 454(7202):297-301.
682 4. Gligoris TG*, et al.* (2014) Closing the cohesin ring: structure and function of its Smc3-
683 kleisin interface. *Science* 346(6212):963-967.
684 5. Lengronne A*, et al.* (2004) Cohesin relocation from sites of chromosomal loading to
685 places of convergent transcription. *Nature* 430(6999):573-578.
686 6. Glynn EF*, et al.* (2004) Genome-wide mapping of the cohesin complex in the yeast
687 *Saccharomyces cerevisiae*. *PLoS Biol* 2(9):e259.
688 7. Schalbetter SA, Fudenberg G, Baxter J, Pollard KS, & Neale MJ (2019) Principles of
689 meiotic chromosome assembly revealed in *S. cerevisiae*. *Nat Commun* 10(1):4795.
690 8. Dauban L*, et al.* (2020) Regulation of cohesin-mediated chromosome folding by Eco1
691 and other partners. *Mol Cell* 77(6):1279-1293.
692 9. Costantino L, Hsieh TS, Lamothe R, Darzacq X, & Koshland D (2020) Cohesin
693 residency determines chromatin loop patterns. *eLife* 9:e59889.
694 10. Oomen ME, Hedger AK, Watts JK, & Dekker J (2020) Detecting chromatin interactions
695 between and along sister chromatids with SisterC. *Nat Methods* 17(10):1002-1009.
696 11. Hadjur S*, et al.* (2009) Cohesins form chromosomal *cis*-interactions at the
697 developmentally regulated *IFNG* locus. *Nature* 460(7253):410-413.
698 12. Rao SSP*, et al.* (2017) Cohesin loss eliminates all loop domains. *Cell* 171(2):305-320
699 e324.
700 13. Mitter M*, et al.* (2020) Conformation of sister chromatids in the replicated human
701 genome. *Nature* 586(7827):139-144.
702 14. Rolef Ben-Shahar T*, et al.* (2008) Eco1-dependent cohesin acetylation during
703 establishment of sister chromatid cohesion. *Science* 321(5888):563-566.
704 15. Ünal E*, et al.* (2008) A molecular determinant for the establishment of sister chromatid
705 cohesion. *Science* 321(5888):566-569.
706 16. Beckouët F*, et al.* (2016) Releasing activity disengages cohesin's Smc3/Scc1 interface in
707 a process blocked by acetylation. *Mol Cell* 61(4):563-574.
708 17. Rowland BD*, et al.* (2009) Building sister chromatid cohesion: Smc3 acetylation
709 counteracts an antiestablishment activity. *Mol Cell* 33(6):763-774.
710 18. Sutani T, Kawaguchi T, Kanno R, Itoh T, & Shirahige K (2009) Budding yeast
711 Wpl1(Rad61)-Pds5 complex counteracts sister chromatid cohesion-establishing reaction.
712 *Curr Biol* 19(6):492-497.
713 19. Lengronne A*, et al.* (2006) Establishment of sister chromatid cohesion at the *S. cerevisiae*
714 replication fork. *Mol Cell* 23(6):787-799.
715 20. D'Ambrosio C*, et al.* (2008) Identification of *cis*-acting sites for condensin loading onto
716 budding yeast chromosomes. *Genes Dev* 22(16):2215-2227.
717 21. Busslinger GA*, et al.* (2017) Cohesin is positioned in mammalian genomes by
718 transcription, CTCF and Wapl. *Nature* 544(7651):503-507.
719 22. Ocampo-Hafalla M, Muñoz S, Samora CP, & Uhlmann F (2016) Evidence for cohesin
720 sliding along budding yeast chromosomes. *Open Biol* 6(6):e150178.

721 23. Bausch C, *et al.* (2007) Transcription alters chromosomal locations of cohesin in
722 *Saccharomyces cerevisiae*. *Mol Cell Biol* 27(24):8522-8532.
723 24. Davidson IF, *et al.* (2016) Rapid movement and transcriptional re-localization of human
724 cohesin on DNA. *EMBO J* 35(24):2671-2685.
725 25. Stigler J, Çamdere GO, Koshland DE, & Greene EC (2016) Single-molecule imaging
726 reveals a collapsed conformational state for DNA-bound cohesin. *Cell Rep* 15(5):988-
727 998.
728 26. Kanke M, Tahara E, Huis In't Veld PJ, & Nishiyama T (2016) Cohesin acetylation and
729 Wapl-Pds5 oppositely regulate translocation of cohesin along DNA. *EMBO J*
730 35(24):2686-2698.
731 27. Davidson IF, *et al.* (2019) DNA loop extrusion by human cohesin. *Science*
732 366(6471):1338-1345.
733 28. Kim Y, Shi Z, Zhang H, Finkelstein IJ, & Yu H (2019) Human cohesin compacts DNA
734 by loop extrusion. *Science* 366(6471):1345-1349.
735 29. Sanborn AL, *et al.* (2015) Chromatin extrusion explains key features of loop and domain
736 formation in wild-type and engineered genomes. *Proc Natl Acad Sci U S A*
737 112(47):e6456-6465.
738 30. Fudenberg G, *et al.* (2016) Formation of chromosomal domains by loop extrusion. *Cell*
739 *Rep* 15(9):2038-2049.
740 31. Nasmyth K (2001) Disseminating the genome: joining, resolving, and separating sister
741 chromatids during mitosis and meiosis. *Annu Rev Genet* 35:673-745.
742 32. Wutz G, *et al.* (2017) Topologically associating domains and chromatin loops depend on
743 cohesin and are regulated by CTCF, WAPL, and PDS5 proteins. *EMBO J* 36(24):3573-
744 3599.
745 33. Haarhuis JHI, *et al.* (2017) The cohesin release factor WAPL restricts chromatin loop
746 extension. *Cell* 169(4):693-707.
747 34. Gassler J, *et al.* (2017) A mechanism of cohesin-dependent loop extrusion organizes
748 zygotic genome architecture. *EMBO J* 36(24):3600-3618.
749 35. Borrie MS, Campor JS, Joshi H, & Gartenberg MR (2017) Binding, sliding, and function
750 of cohesin during transcriptional activation. *Proc Natl Acad Sci U S A* 114(7):e1062.
751 36. Brickner JH & Walter P (2004) Gene recruitment of the activated *INO1* locus to the
752 nuclear membrane. *PLoS Biol* 2(11):e342.
753 37. Karaboja X, *et al.* (2021) XerD unloads bacterial SMC complexes at the replication
754 terminus. *Mol Cell* 81(4):756-766.
755 38. Shaner NC, *et al.* (2004) Improved monomeric red, orange and yellow fluorescent
756 proteins derived from *Discosoma* sp. red fluorescent protein. *Nat Biotechnol*
757 22(12):1567-1572.
758 39. Shemiakina, I.I., *et al.* (2012) A monomeric red fluorescent protein with low cytotoxicity.
759 *Nat Commun* 3:1204.
760 40. Shu X, Shaner NC, Yarbrough CA, Tsien RY, & Remington SJ (2006) Novel
761 chromophores and buried charges control color in mFruits. *Biochemistry* 45(32):9639-
762 9647.
763 41. Verma R, *et al.* (1997) Phosphorylation of Sic1p by G1 Cdk required for its degradation
764 and entry into S phase. *Science* 278(5337):455-460.

765 42. Guacci V, Koshland D, & Strunnikov A (1997) A direct link between sister chromatid
766 cohesion and chromosome condensation revealed through the analysis of *MCD1* in *S.*
767 *cerevisiae*. *Cell* 91(1):47-57.
768 43. Michaelis C, Ciosk R, & Nasmyth K (1997) Cohesins: chromosomal proteins that prevent
769 premature separation of sister chromatids. *Cell* 91(1):35-45.
770 44. Hu B*, et al.* (2015) Biological chromodynamics: a general method for measuring protein
771 occupancy across the genome by calibrating ChIP-seq. *Nucleic Acids Res* 43(20):e132.
772 45. Eng T, Guacci V, & Koshland D (2014) ROCC, a conserved region in cohesin's Mcd1
773 subunit, is essential for the proper regulation of the maintenance of cohesion and
774 establishment of condensation. *Mol Biol Cell* 25(16):2351-2364.
775 46. Haering CH*, et al.* (2004) Structure and stability of cohesin's Smc1-kleisin interaction.
776 *Mol Cell* 15(6):951-964.
777 47. Ünal E, Heidinger-Pauli JM, & Koshland D (2007) DNA double-strand breaks trigger
778 genome-wide sister-chromatid cohesion through Eco1 (Ctf7). *Science* 317(5835):245-
779 248.
780 48. Chan KL*, et al.* (2012) Cohesin's DNA exit gate is distinct from its entrance gate and is
781 regulated by acetylation. *Cell* 150(5):961-974.
782 49. Lopez-Serra L, Lengronne A, Borges V, Kelly G, & Uhlmann F (2013) Budding yeast
783 Wapl controls sister chromatid cohesion maintenance and chromosome condensation.
784 *Curr Biol* 23(1):64-69.
785 50. Srinivasan M*, et al.* (2019) Scc2 counteracts a Wapl-independent mechanism that
786 releases cohesin from chromosomes during G1. *eLife* 8.
787 51. Çamdere G, Guacci V, Stricklin J, & Koshland D (2015) The ATPases of cohesin
788 interface with regulators to modulate cohesin-mediated DNA tethering. *eLife* 4:e11315.
789 52. Elbatsh AM*, et al.* (2016) Cohesin releases DNA through asymmetric ATPase-driven
790 ring opening. *Mol Cell* 61(4):575-588.
791 53. Bloom MS, Koshland D, & Guacci V (2018) Cohesin function in cohesion, condensation,
792 and DNA repair is regulated by Wpl1p via a common mechanism in *Saccharomyces*
793 *cerevisiae*. *Genetics* 208(1):111-124.
794 54. Guacci V*, et al.* (2015) A novel mechanism for the establishment of sister chromatid
795 cohesion by the *ECO1* acetyltransferase. *Mol Biol Cell* 26(1):117-133.
796 55. Zhang Y*, et al.* (2019) The fundamental role of chromatin loop extrusion in physiological
797 V(D)J recombination. *Nature* 573(7775):600-604.
798 56. Collier JE*, et al.* (2020) Transport of DNA within cohesin involves clamping on top of
799 engaged heads by Scc2 and entrapment within the ring by Scc3. *eLife* 9:e59560.
800 57. Higashi TL*, et al.* (2020) A structure-based mechanism for DNA entry into the cohesin
801 ring. *Mol Cell* 79(6):917-933 e919.
802 58. Shi Z, Gao H, Bai XC, & Yu H (2020) Cryo-EM structure of the human cohesin-NIPBL-
803 DNA complex. *Science* 368(6498):1454-1459.
804 59. Srinivasan M*, et al.* (2018) The cohesin ring uses its hinge to organize DNA using non-
805 topological as well as topological mechanisms. *Cell* 173(6):1508-1519.
806 60. Bauer BW*, et al.* (2021) Cohesin mediates DNA loop extrusion by a "swing and clamp"
807 mechanism. *Cell* 184(21):5448-5464 e5422.
808 61. Murayama Y & Uhlmann F (2014) Biochemical reconstitution of topological DNA
809 binding by the cohesin ring. *Nature* 505(7483):367-371.

810 62. Petela NJ, *et al.* (2018) Scc2 is a potent activator of cohesin's ATPase that promotes
811 loading by binding Scc1 without Pds5. *Mol Cell* 70(6):1134-1148.
812 63. Bastie N, *et al.* (2021) Smc3 acetylation, Pds5 and Scc2 control the translocase activity
813 that establishes cohesin dependent chromatin loops. *BioRXiv*
814 https://doi.org/10.1101/2021.04.21.440823.
815 64. Pradhan B, *et al.* (2021) SMC complexes can traverse physical roadblocks bigger than
816 their ring size. *BioRXiv* https://doi.org/10.1101/2021.07.15.452501.
817 65. Wutz G, *et al.* (2020) ESCO1 and CTCF enable formation of long chromatin loops by
818 protecting cohesin(STAG1) from WAPL. *eLife* 9:e52091.
819 66. Barton RE, Massari LF, Robertson D, & Marston AL (2022) Eco1-dependent cohesin
820 acetylation anchors chromatin loops and cohesion to define functional meiotic
821 chromosome domains. *eLife* 11.
822 67. Vian L, *et al.* (2018) The energetics and physiological impact of cohesin extrusion. *Cell*
823 173(5):1165-1178.
824 68. Krietenstein N, *et al.* (2020) Ultrastructural details of mammalian chromosome
825 architecture. *Mol Cell* 78(3):554-565 e557.
826 69. Chou CC, Patel MT, & Gartenberg MR (2015) A series of conditional shuttle vectors for
827 targeted genomic integration in budding yeast. *FEMS Yeast Res* 15(3):fov010.
828 70. Morawska M & Ulrich HD (2013) An expanded tool kit for the auxin-inducible degron
829 system in budding yeast. *Yeast* 30(9):341-351.
830 71. Tanaka S, Miyazawa-Onami M, Iida T, & Araki H (2015) iAID: an improved auxin-
831 inducible degron system for the construction of a 'tight' conditional mutant in the budding
832 yeast *Saccharomyces cerevisiae*. *Yeast* 32(8):567-581.
833 72. Huang L, Pike D, Sleat DE, Nanda V, & Lobel P (2014) Potential pitfalls and solutions
834 for use of fluorescent fusion proteins to study the lysosome. *PLoS One* 9(2):e88893.
835 73. Zacharias DA, Violin JD, Newton AC, & Tsien RY (2002) Partitioning of lipid-modified
836 monomeric GFPs into membrane microdomains of live cells. *Science* 296(5569):913-
837 916.
838 74. Lew DJ & Reed SI (1993) Morphogenesis in the yeast cell cycle: regulation by Cdc28
839 and cyclins. *J Cell Biol* 120(6):1305-1320.
840

Borrie and Gartenberg, 2022
Figure 1

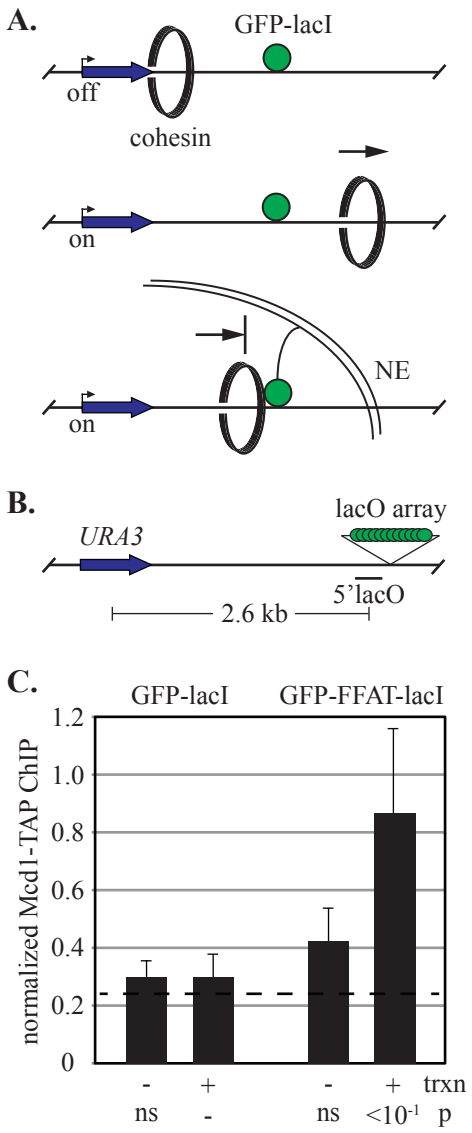

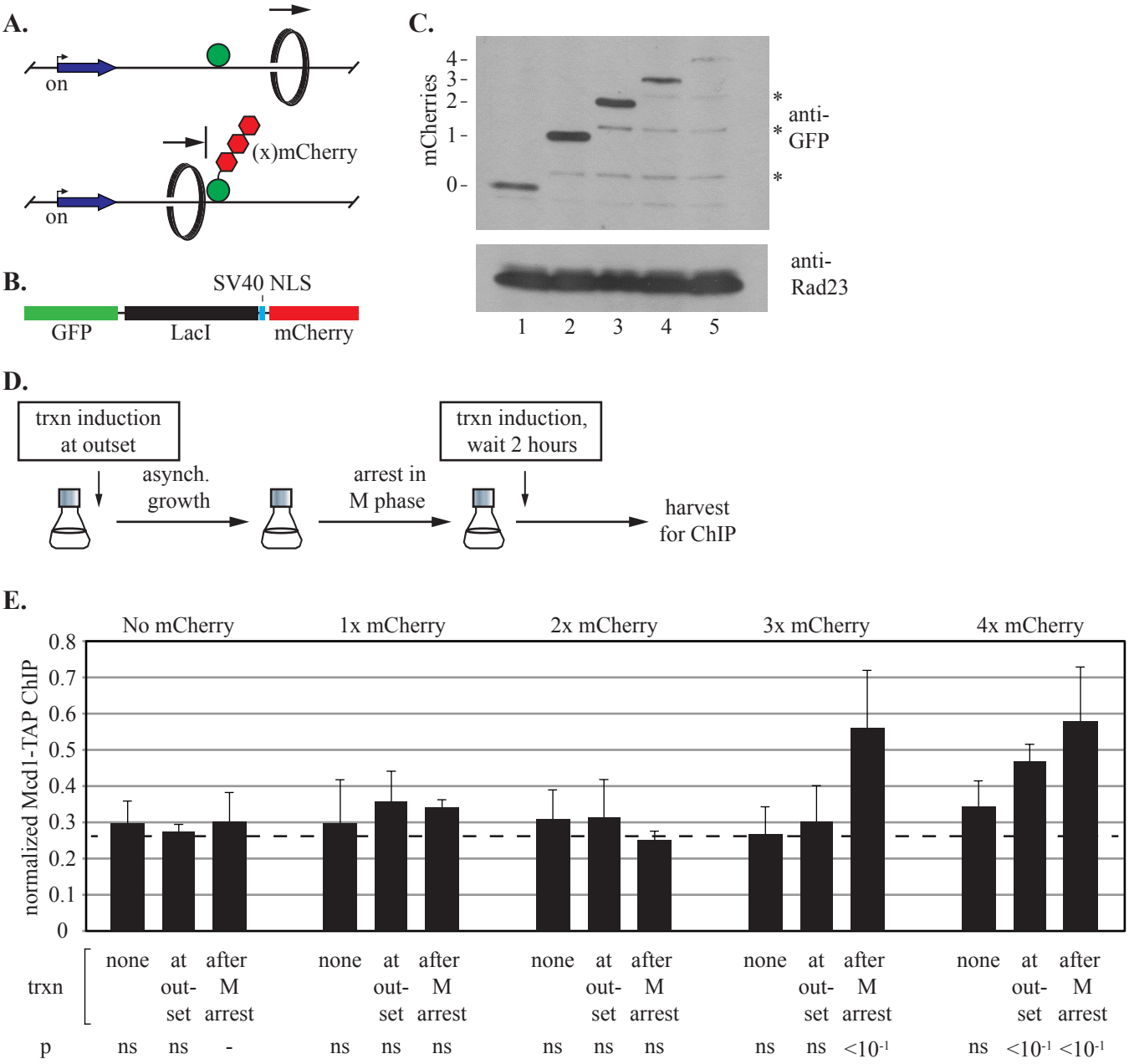
A.
on
(x)mCherry
on
B.
SV40 NLS
GFP
LacI
mCherry
C.
mCherries
4 -
3 -
2 -
1 -
0 -
anti-
GFP
anti-
Rad23
1 2 3 4 5
D.
trxn induction
at outset
asynch.
growth
arrest in
M phase
trxn induction,
wait 2 hours
harvest
for ChIP
E.
No mCherry
1x mCherry
2x mCherry
3x mCherry
4x mCherry
normalized Mcd1-TAP ChIP
0.8
0.7
0.6
0.5
0.4
0.3
0.2
0.1
0
trxn
none
at out-set
after M arrest
p
ns
ns
-
ns
ns
ns
ns
ns
ns
ns
ns
<10-1
ns
<10-1
<10-1

Borrie and Gartenberg, 2022
Figure 3

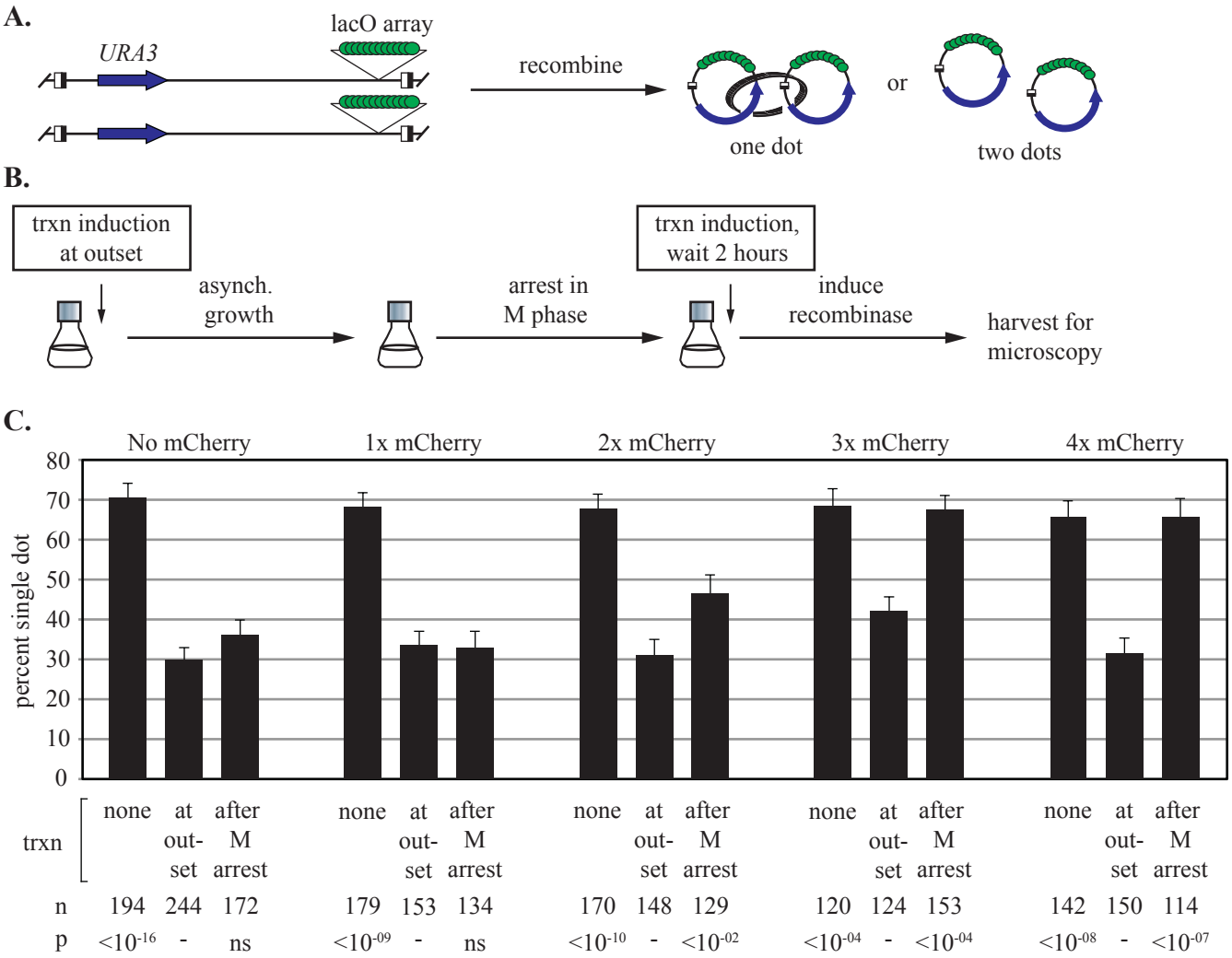

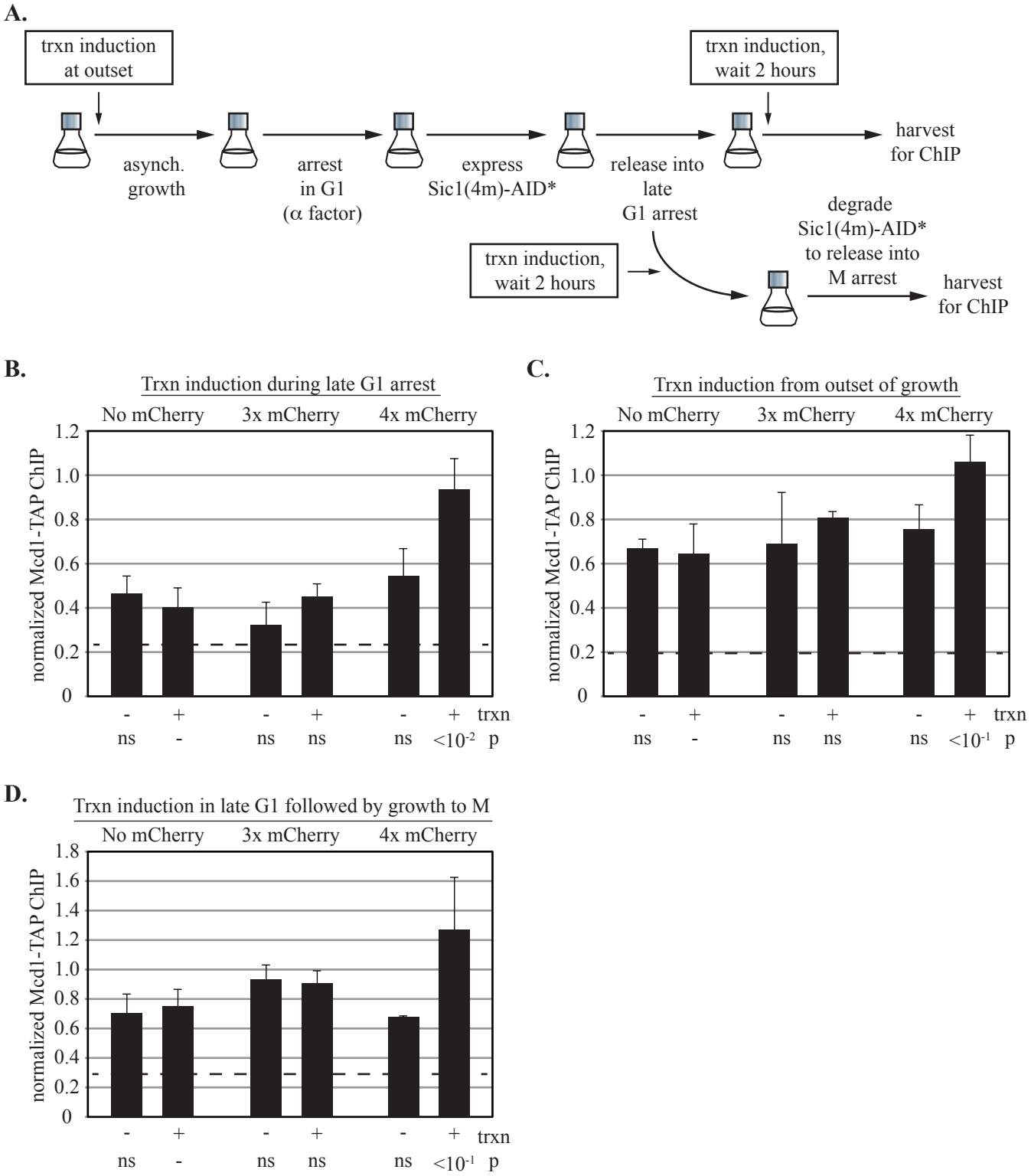
A.
trxn induction at outset
asynch. growth
arrest in G1 (α factor)
express Sic1(4m)-AID*
release into late G1 arrest
trxn induction, wait 2 hours
harvest for ChIP
trxn induction, wait 2 hours
degrade Sic1(4m)-AID* to release into M arrest
harvest for ChIP
B.
Trxn induction during late G1 arrest
No mCherry
3x mCherry
4x mCherry
normalized Mcd1-TAP ChIP
1.2
1.0
0.8
0.6
0.4
0.2
0
- + - + - + trxn
ns - ns ns ns <10-2 p
C.
Trxn induction from outset of growth
No mCherry
3x mCherry
4x mCherry
normalized Mcd1-TAP ChIP
1.2
1.0
0.8
0.6
0.4
0.2
0
- + - + - + trxn
ns - ns ns ns <10-1 p
D.
Trxn induction in late G1 followed by growth to M
No mCherry
3x mCherry
4x mCherry
normalized Mcd1-TAP ChIP
1.8
1.6
1.4
1.2
1.0
0.8
0.6
0.4
0.2
0
- + - + - + trxn
ns - ns ns ns <10-1 p

Borrie and Gartenberg, 2022
Figure 5

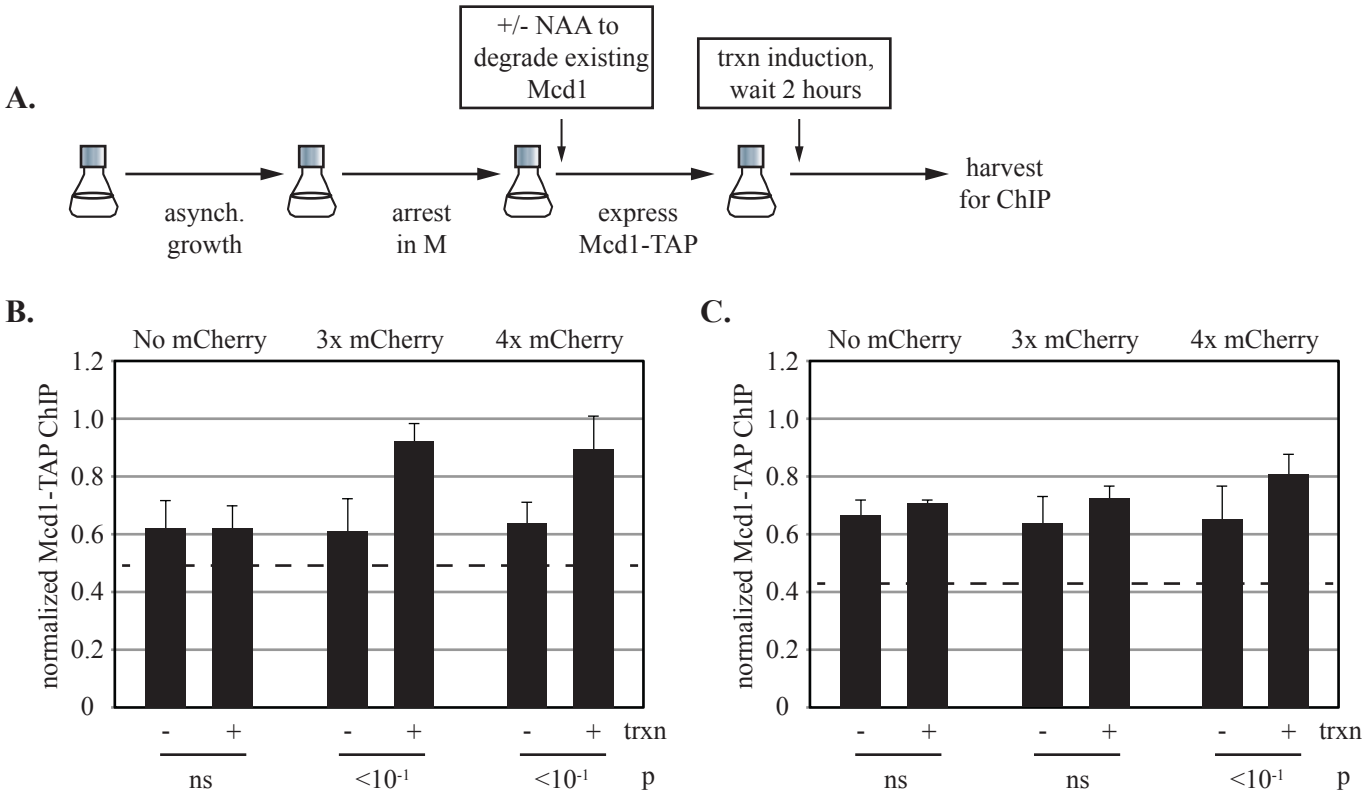

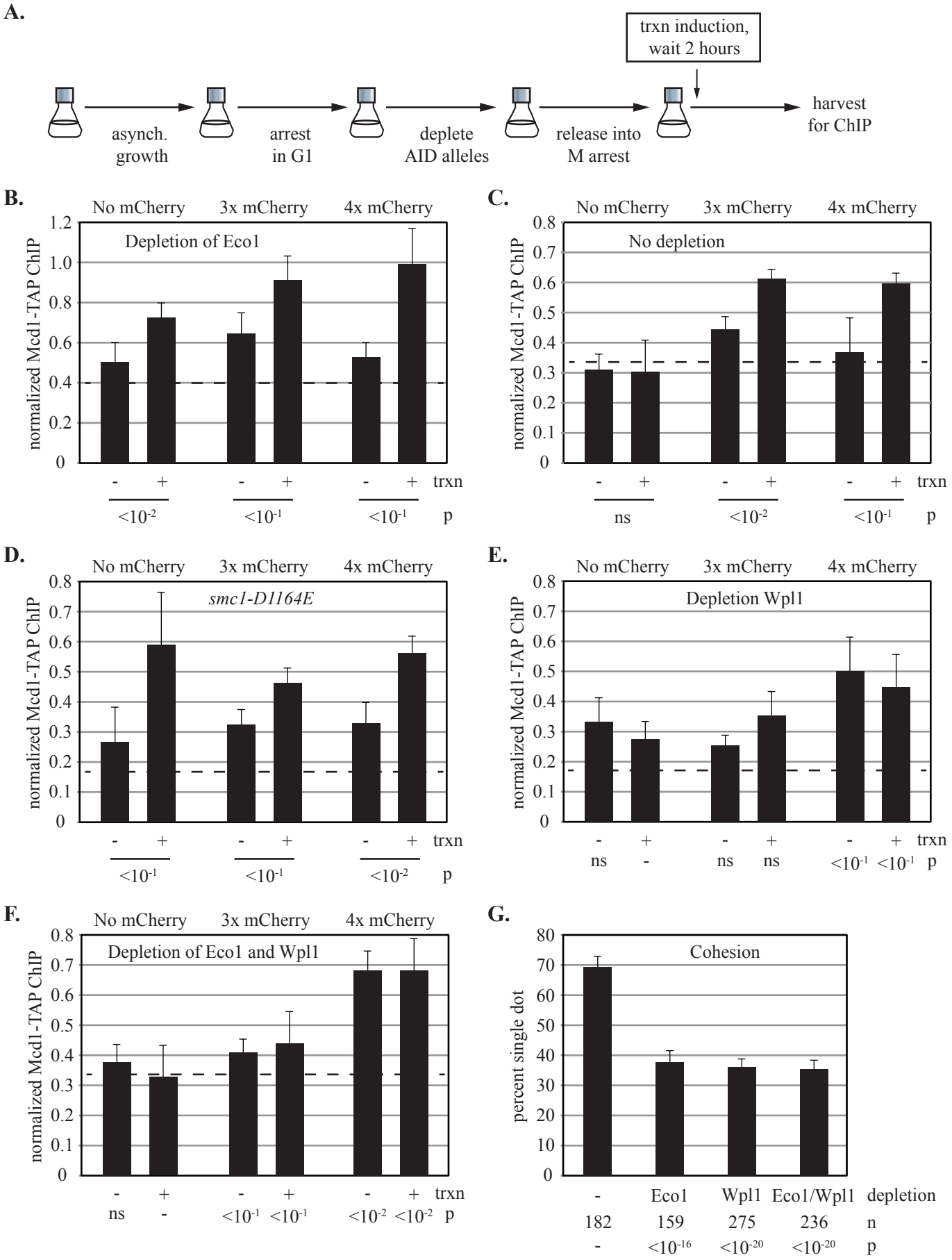
A.
trxn induction, wait 2 hours
asynch. growth
arrest in G1
deplete AID alleles
release into M arrest
harvest for ChIP
B.
No mCherry
3x mCherry
4x mCherry
Depletion of Eco1
normalized Mcd1-TAP ChIP
trxn
p
C.
No depletion
D.
smc1-D1164E
E.
Depletion Wpl1
F.
Depletion of Eco1 and Wpl1
G.
Cohesion
percent single dot
Eco1
Wpl1
Eco1/Wpl1
depletion
n

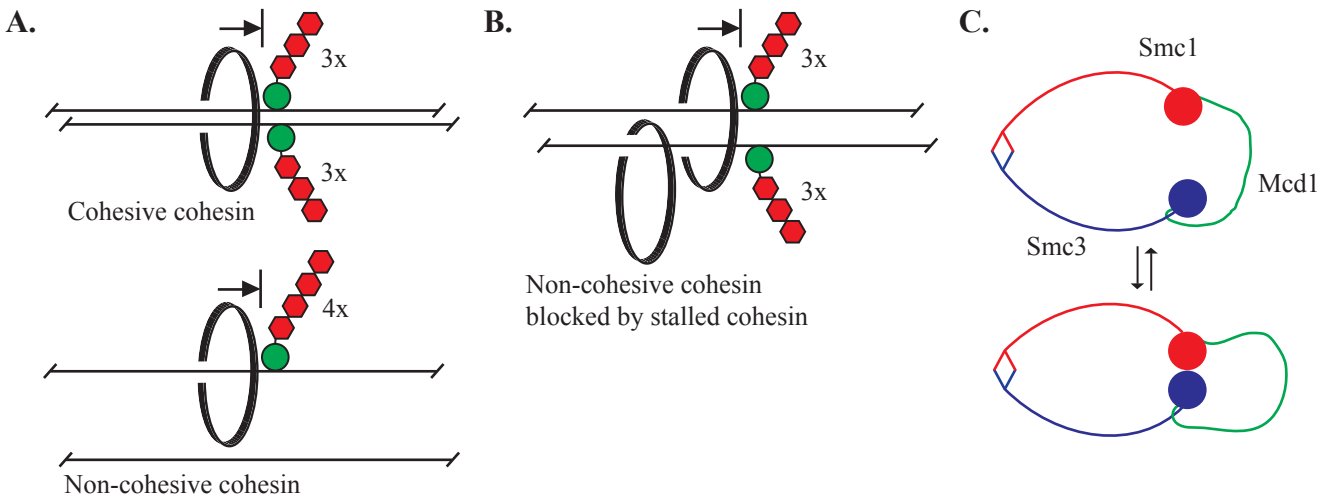
A.
3x
3x
Cohesive cohesin
4x
Non-cohesive cohesin
B.
3x
3x
Non-cohesive cohesin
blocked by stalled cohesin
C.
Smc1
Mcd1
Smc3

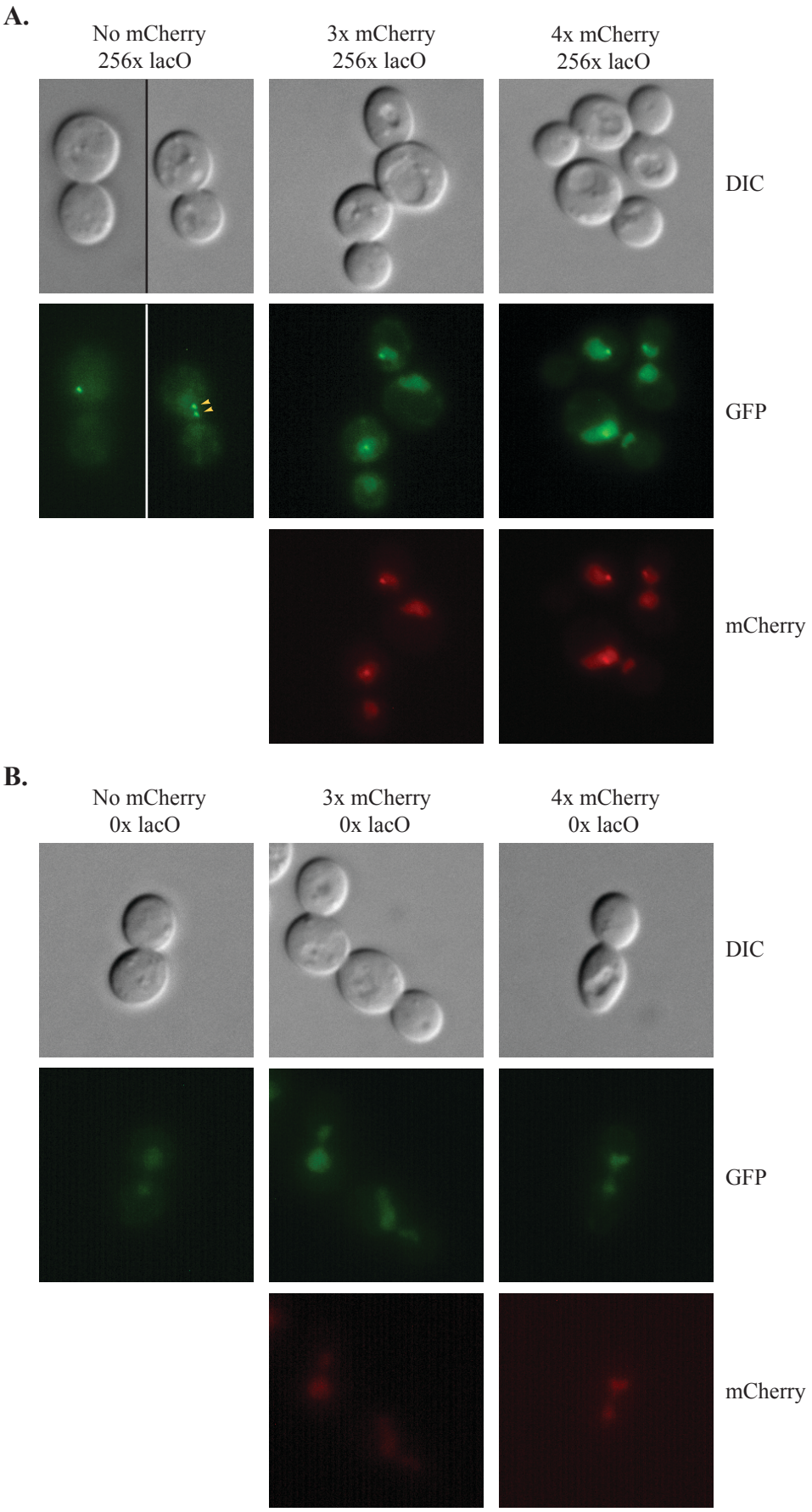
A.
No mCherry
256x lacO
3x mCherry
256x lacO
4x mCherry
256x lacO
DIC
GFP
mCherry
B.
No mCherry
0x lacO
3x mCherry
0x lacO
4x mCherry
0x lacO
DIC
GFP
mCherry

Borrie and Gartenberg, 2021
Figure S2

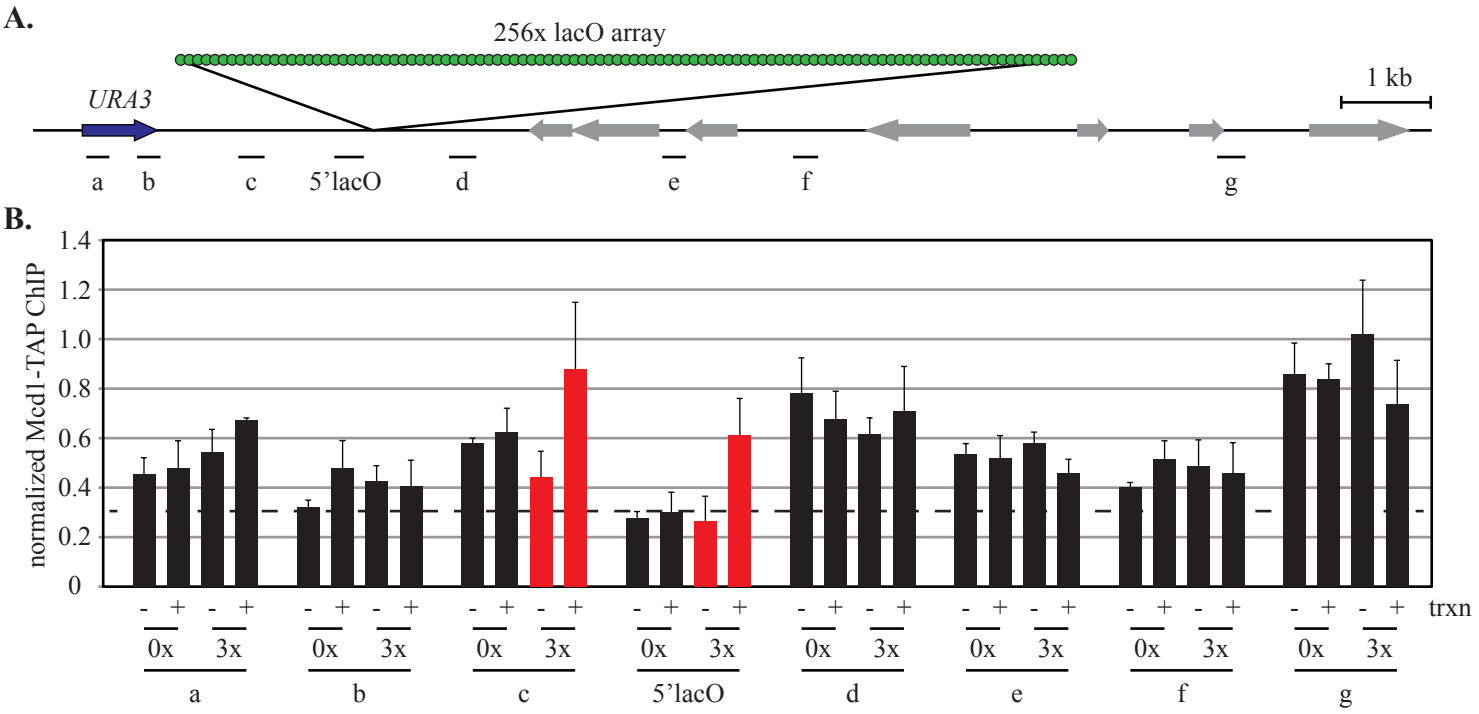

Borrie and Gartenberg, 2022
Figure S3

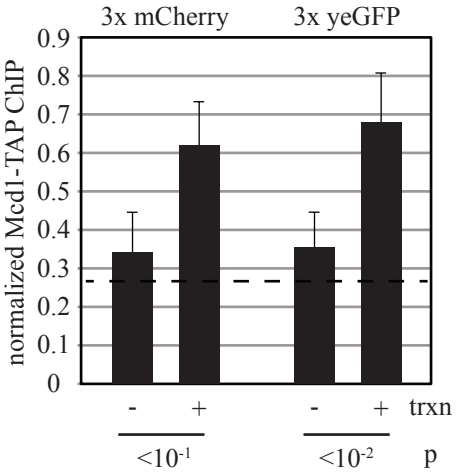

Borrie and Gartenberg, 2022
Figure S4

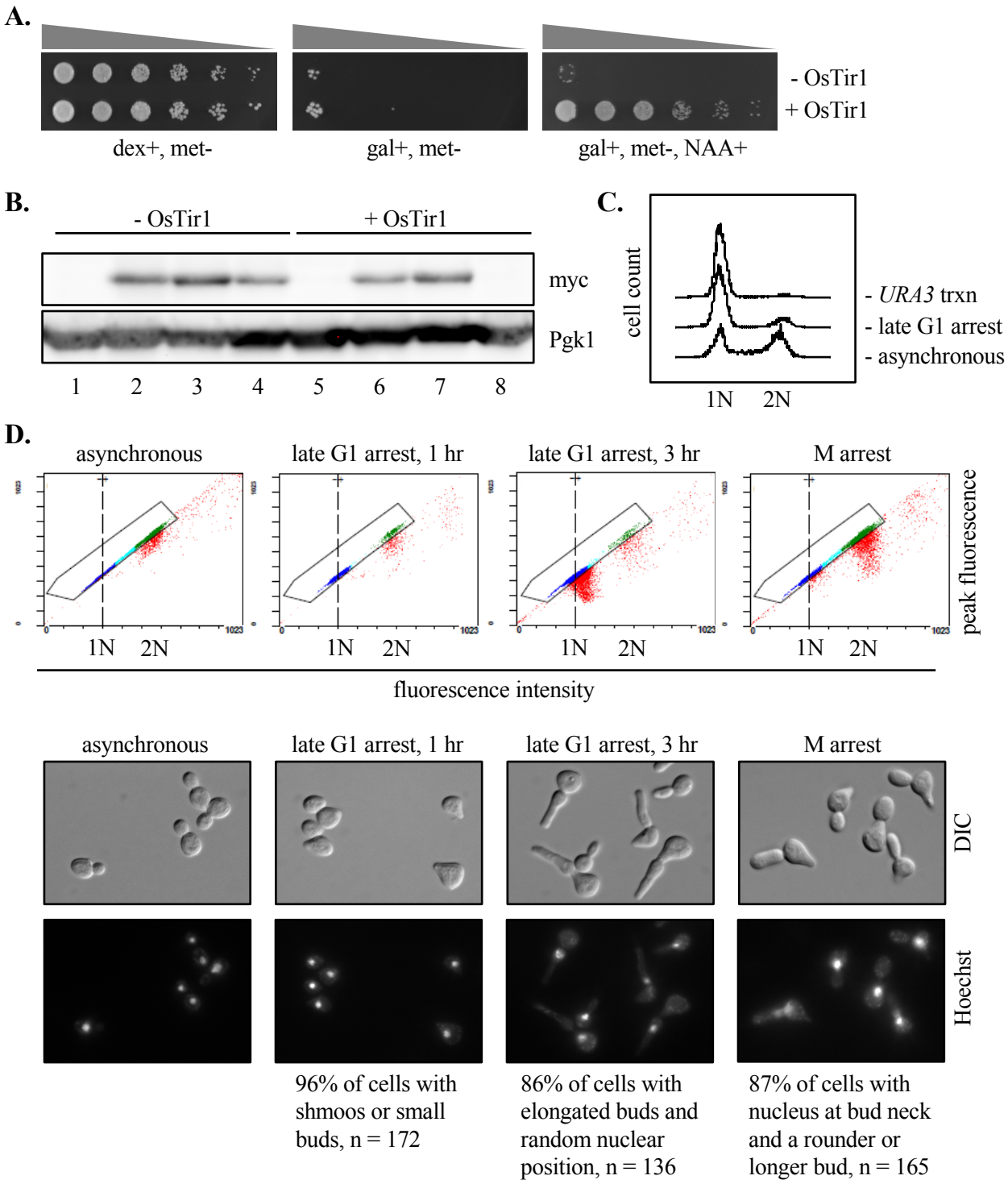

Borrie and Gartenberg, 2022
Figure S5

A.

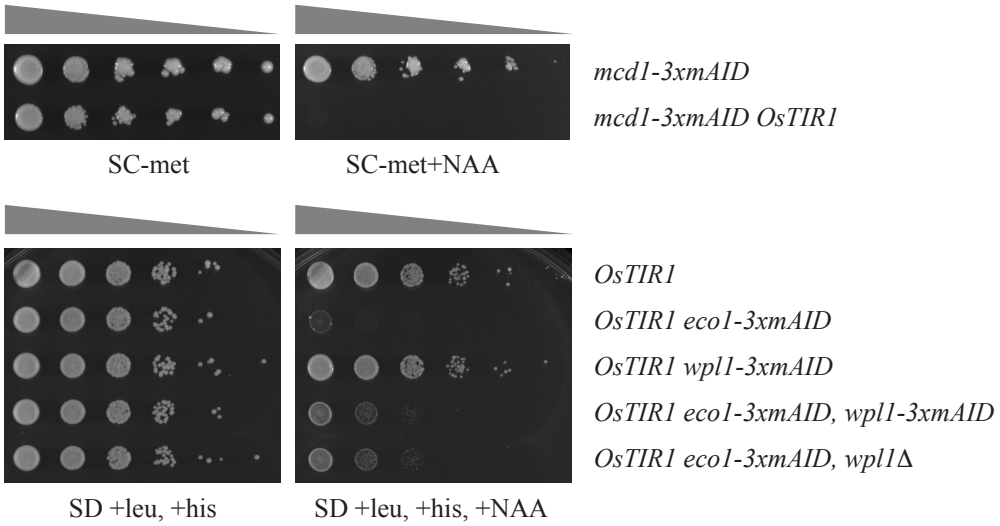

B.

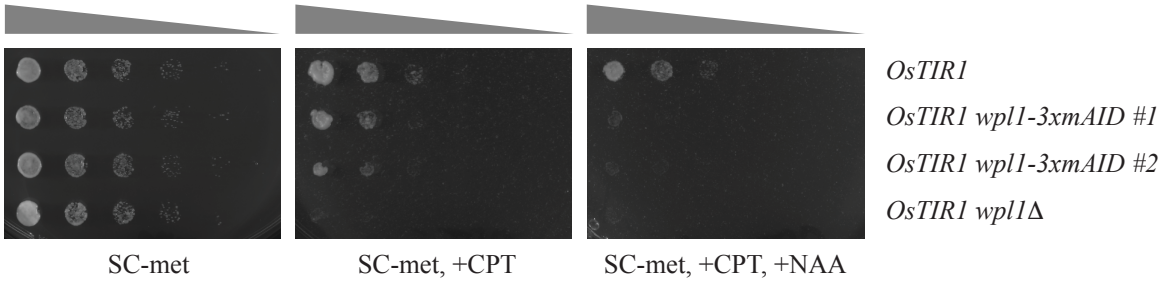

C.

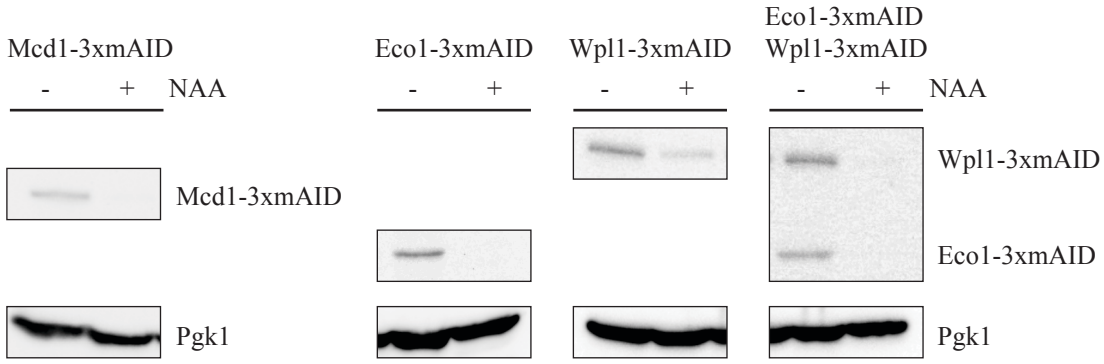

D.

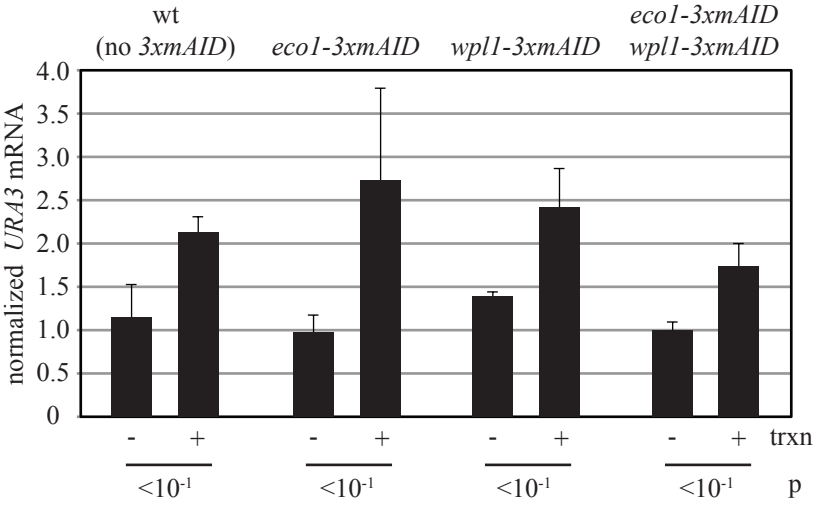

Borrie and Gartenberg, 2022
Figure S6

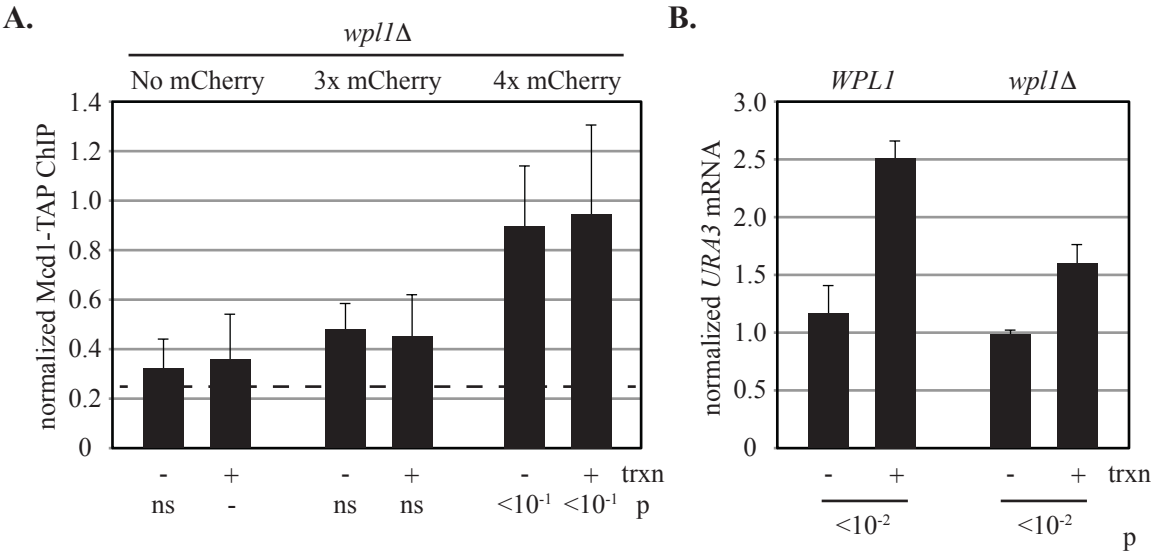

Borrie and Gartenberg, 2022
Figure S7

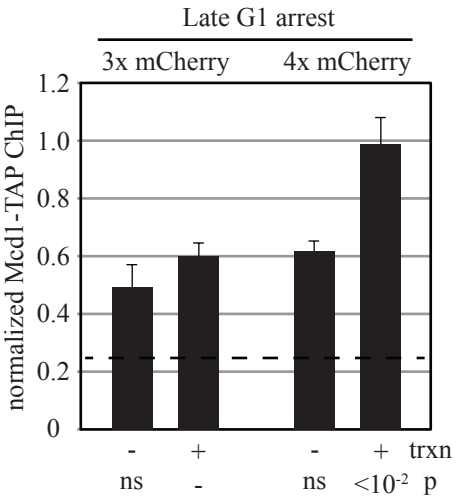

Table S1 – Yeast strains

Name	Genotype	Parent	Ref	Fig.
MSB35.2	*MAT***a** *hmr-git1Δ::RS-URA3f-loxP-256xlacO-RS ade2-1::(HIS3p-GFP-lacI::ADE2)*$_2$ *leu2-3,112::(GAL1p-RecR::LEU2)*$_2$ *cdc20::MET3p-cdc20::loxP can1-100 his3-11,15 trp1-1 ura3-1*	MSB31	Borrie et al 2017	3C, S1A
MSB114	*MAT***a** *hmr-git1Δ::RS-URA3f-loxP-256xlacO-RS ade2-1::(HIS3p-GFP-lacI::ADE2)*$_2$ *leu2-3,112::(GAL1p-RecR::LEU2)*$_2$ *cdc20::MET3p-cdc20::loxP MCD1-TAP::natMX ura3Δ::hphMX can1-100 his3-11,15 trp1-1*	MSB35.2	This study	1C, 2E, S2B
MRG6947	*MAT***a** *hmr-git1Δ::RS-URA3f-loxP-256xlacO-RS leu2-3,112::(GAL1p-RecR::LEU2)*$_2$ *MCD1-TAP::natMX cdc20::MET3p-cdc20::loxP his3-11,15::HIS3p-GFP-FFAT-lacI::ADE2::HIS3p-GFP-FFAT-lacI::HIS3 ura3Δ::AgTEFp-SpHIS5 ade2-1 can1-100 trp1-1*	MRG6767 x MRG6900	“”	1C
MSB174	*MAT***a** *hmr-git1Δ::RS-URA3f-loxP-256xlacO-RS ade2-1::HIS3p-GFP-lacI::ADE2 leu2-3,112::(GAL1p-RecR::LEU2)*$_2$ *ura3Δ::AgTEFp-SpHIS5 bar1Δ can1-100 his3-11,15 trp1-1*	MRG6860	“”	2C
MSB179	*MAT***a** *hmr-git1Δ::RS-URA3f-loxP-256xlacO-RS ade2-1::HIS3p-GFP-lacI-1xmCherry::hphMX::ADE2 leu2-3,112::(GAL1p-RecR::LEU2)*$_2$ *ura3Δ::AgTEFp-SpHIS5 bar1Δ can1-100 his3-11,15 trp1-1*	MSB174	“”	2C
MSB180	*MAT***a** *hmr-git1Δ::RS-URA3f-loxP-256xlacO-RS ade2-1::HIS3p-GFP-lacI-2xmCherry::hphMX::ADE2 leu2-3,112::(GAL1p-RecR::LEU2)*$_2$ *ura3Δ::AgTEFp-SpHIS5 bar1Δ can1-100 his3-11,15 trp1-1*	MSB174	“”	2C
MSB181	*MAT***a** *hmr-git1Δ::RS-URA3f-loxP-256xlacO-RS ade2-1::HIS3p-GFP-lacI-3xmCherry::hphMX::ADE2 leu2-3,112::(GAL1p-RecR::LEU2)*$_2$ *ura3Δ::AgTEFp-SpHIS5 bar1Δ can1-100 his3-11,15 trp1-1*	MSB174	“”	2C
MRG7102	*MAT***a** *hmr-git1Δ::RS-URA3f-loxP-256xlacO-RS ade2-1::HIS3p-GFP-lacI-4xmCherry::kanMX::ADE2 leu2-3,112::(GAL1p-RecR::LEU2)*$_2$ *ura3Δ::AgTEFp-SpHIS5 bar1Δ can1-100 his3-11,15 trp1-1*	MSB181	“”	2C
MRG6810	*MAT***a** *hmr-git1Δ::RS-URA3f-loxP-256xlacO-RS ade2-1::HIS3p-GFP-lacI-*	MSB164	“”	2E

	1xmCherry::hphMX::ADE2::HIS3p-GFP-lacI::ADE2 leu2-3,112::(GAL1p-RecR::LEU2)$_2$ cdc20::MET3p-cdc20::loxP MCD1-TAP::natMX ura3Δ::AgTEFp-SpHIS5 can1-100 his3-11,15 trp1-1			
MRG6812	*MAT***a** *hmr-git1Δ::RS-URA3f-loxP-256xlacO-RS ade2-1::HIS3p-GFP-lacI-2xmCherry::hphMX::ADE2::HIS3p-GFP-lacI::ADE2 leu2-3,112::(GAL1p-RecR::LEU2)$_2$ loxP::MET3p-cdc20 MCD1-TAP::natMX ura3Δ::AgTEFp-SpHIS5 can1-100 his3-11,15 trp1-1*	MSB164	“”	2E
MSB165.1	*MAT***a** *hmr-git1Δ::RS-URA3f-loxP-256xlacO-RS ade2-1::HIS3p-GFP-lacI-3xmCherry::hphMX::ADE2::HIS3p-GFP-lacI::ADE2 leu2-3,112::(GAL1p-RecR::LEU2)$_2$ cdc20::MET3p-cdc20::loxP MCD1-TAP::natMX ura3Δ::AgTEFp-SpHIS5 can1-100 his3-11,15 trp1-1*	MSB164	“”	2E, S2B, S3
MRG7060	*MAT***a** *hmr-git1Δ::RS-URA3f-loxP-256xlacO-RS ade2-1::HIS3p-GFP-lacI-4xmCherry::kanMX::ADE2::HIS3p-GFP-lacI::ADE2 leu2-3,112::(GAL1p-RecR::LEU2)$_2$ cdc20::MET3p-cdc20::loxP MCD1-TAP::natMX ura3Δ::AgTEFp-SpHIS5 can1-100 his3-11,15 trp1-1*	MSB165.1	“”	2E, 3C, S1A
MRG6806	*MAT***a** *hmr-git1Δ::RS-URA3f-loxP-256xlacO-RS ade2-1::HIS3p-GFP-lacI-1xmCherry::hphMX::ADE2::HIS3p-GFP-lacI::ADE2 leu2-3,112::(GAL1p-RecR::LEU2)$_2$ cdc20::MET3p-cdc20::loxP can1-100 his3-11,15 trp1-1 ura3-1*	MSB35.2	“”	3C
MRG6808	*MAT***a** *hmr-git1Δ::RS-URA3f-loxP-256xlacO-RS ade2-1::HIS3p-GFP-lacI-2xmCherry::hphMX::ADE2::HIS3p-GFP-lacI::ADE2 leu2-3,112::(GAL1p-RecR::LEU2)$_2$ cdc20::MET3p-cdc20::loxP can1-100 his3-11,15 trp1-1 ura3-1*	MSB35.2	“”	3C
MSB167	*MAT***a** *hmr-git1Δ::RS-URA3f-loxP-256xlacO-RS ade2-1::HIS3p-GFP-lacI-3xmCherry::hphMX::ADE2::HIS3p-GFP-lacI::ADE2 leu2-3,112::(GAL1p-RecR::LEU2)$_2$ cdc20::MET3p-cdc20::loxP can1-100 his3-11,15 trp1-1 ura3-1*	MSB165.1 x W303-1B	“”	3C, S1A
MRG7027	*MAT***a** *hmr-git1Δ::RS-URA3f-loxP-256xlacO-RS ade2-1::(HIS3p-GFP-lacI::ADE2)$_2$ leu2-3,112::GAL1p-SIC1(4m)-AID*-9xmyc::LEU2 cdc20::MET3p-cdc20::loxP MCD1-TAP::natMX*	MRG7013	“”	4B, 4C, S4A, S4B,

	ura3Δ::AgTEFp-SpHIS5 bar1Δ can1-100 his3-11,15 trp1-1			S4C, S7B
MRG7026	*MAT***a** *hmr-git1Δ::RS-URA3f-loxP-256xlacO-RS ade2-1::HIS3p-GFP-lacI-3xmCherry::hphMX::ADE2::HIS3p-GFP-lacI::ADE2 leu2-3,112::GAL1p-SIC1(4m)-AID*-9xmyc::LEU2 cdc20::MET3p-cdc20::loxP MCD1-TAP::natMX ura3Δ::AgTEFp-SpHIS5 bar1Δ can1-100 his3-11,15 trp1-1*	MRG7015	“”	4B, 4C
MRG7059	*MAT***a** *hmr-git1Δ::RS-URA3f-loxP-256xlacO-RS ade2-1::HIS3p-GFP-lacI-4xmCherry::kanMX::ADE2::HIS3p-GFP-lacI::ADE2 leu2-3,112::GAL1p-SIC1(4m)-AID*-9xmyc::LEU2 cdc20::MET3p-cdc20::loxP MCD1-TAP::natMX ura3Δ::AgTEFp-SpHIS5 bar1Δ can1-100 his3-11,15 trp1-1*	MRG7026	“”	4B, 4C
MRG7033	*MAT***a** *hmr-git1Δ::RS-URA3f-loxP-256xlacO-RS ade2-1::(HIS3p-GFP-lacI::ADE2)$_2$ leu2-3,112::GAL1p-SIC1(4m)-AID*-9xmyc::LEU2 cdc20::MET3p-cdc20::loxP MCD1-TAP::natMX trp1-1::CgTRP1-ADH1p-OsTIR1-CaADH1t ura3Δ::AgTEFp-SpHIS5 bar1Δ can1-100 his3-11,15*	MRG7027	“”	4D, S4A, S4B, S4D
MRG7032	*MAT***a** *hmr-git1Δ::RS-URA3f-loxP-256xlacO-RS ade2-1::HIS3p-GFP-lacI-3xmCherry::hphMX::ADE2::HIS3p-GFP-lacI::ADE2 leu2-3,112::GAL1p-SIC1(4m)-AID*-9xmyc::LEU2 cdc20::MET3p-cdc20::loxP MCD1-TAP::natMX trp1-1::CgTRP1-ADH1p-OsTIR1-CaADH1t ura3Δ::AgTEFp-SpHIS5 bar1Δ can1-100 his3-11,15*	MRG7026	“”	4D
MRG7282	*MAT***a** *hmr-git1Δ::RS-URA3f-loxP-256xlacO-RS ade2-1::HIS3p-GFP-lacI-4xmCherry::kanMX::ADE2::HIS3p-GFP-lacI::ADE2 leu2-3,112::GAL1p-SIC1(4m)-AID*-9xmyc::LEU2 cdc20::MET3p-cdc20::loxP MCD1-TAP::natMX trp1-1::CgTRP1-ADH1p-OsTIR1-CaADH1t ura3Δ::AgTEFp-SpHIS5 bar1Δ can1-100 his3-11,15*	MRG7059	“”	4D
MRG6989	*MAT***a** *hmr-git1Δ::RS-URA3f-loxP-256xlacO-RS ade2-1::(HIS3p-GFP-lacI::ADE2)$_2$ cdc20::MET3p-cdc20::loxP ho::GAL1p-MCD1(R180D,R268D)-TAP::natMX::ho ura3Δ::AgTEFp-SpHIS5 bar1Δ can1-100 his3-11,15 leu2-3,112 trp1-1*	MRG6974 x MRG6963	“”	5B
MRG7294	*MAT***a** *hmr-git1Δ::RS-URA3f-loxP-256xlacO-RS ade2-1::HIS3p-GFP-lacI-*	MRG7290	“”	5B

	3xmCherry::hphMX::ADE2::HIS3p-GFP-lacI::ADE2 cdc20::MET3p-cdc20::loxP ho::GAL1p-MCD1(R180D,R268D)-TAP::natMX::ho ura3Δ::AgTEFp-SpHIS5 bar1Δ can1-100 his3-11,15 leu2-3,112 trp1-1			
MRG7292	*MAT**a** hmr-git1Δ::RS-URA3f-loxP-256xlacO-RS ade2-1::HIS3p-GFP-lacI-4xmCherry::kanMX::ADE2::HIS3p-GFP-lacI::ADE2 cdc20::MET3p-cdc20::loxP ho::GAL1p-MCD1(R180D,R268D)-TAP::natMX::ho ura3Δ::AgTEFp-SpHIS5 bar1Δ can1-100 his3-11,15 leu2-3,112 trp1-1*	MRG7288	“”	5B
MRG7317.1	*MAT**a** hmr-git1Δ::RS-URA3f-loxP-256xlacO-RS ade2-1::(HIS3p-GFP-lacI::ADE2)$_2$ ho::GAL1p-MCD1(R180D,R268D)-TAP::natMX::ho mcd1-3xmAID-5xflag::bleMX trp1-1::CgTRP1-ADH1p-OsTIR1-CaADH1t cdc20::MET3p-cdc20::loxP ura3Δ::AgTEFp-SpHIS5 bar1Δ can1-100 his3-11,15 leu2-3,112*	MRG7312.1	“”	5C, S5A S5C
MRG7319.1	*MAT**a** hmr-git1Δ::RS-URA3f-loxP-256xlacO-RS ade2-1::HIS3p-GFP-lacI-3xmCherry::hphMX::ADE2::HIS3p-GFP-lacI::ADE2 ho::GAL1p-MCD1(R180D,R268D)-TAP::natMX::ho mcd1-3xmAID-5xflag::bleMX trp1-1::CgTRP1-ADH1p-OsTIR1-CaADH1t cdc20::MET3p-cdc20::loxP ura3Δ::AgTEFp-SpHIS5 bar1Δ can1-100 his3-11,15 leu2-3,112*	MRG7316.1	“”	5C
MRG7318.1	*MAT**a** hmr-git1Δ::RS-URA3f-loxP-256xlacO-RS ade2-1::HIS3p-GFP-lacI-4xmCherry::kanMX::ADE2::HIS3p-GFP-lacI::ADE2 ho::GAL1p-MCD1(R180D,R268D)-TAP::natMX::ho mcd1-3xmAID-5xflag::bleMX trp1-1::CgTRP1-ADH1p-OsTIR1-CaADH1t cdc20::MET3p-cdc20::loxP ura3Δ::AgTEFp-SpHIS5 bar1Δ can1-100 his3-11,15 leu2-3,112*	MRG7315.1	“”	5C
MRG7301.1	*MAT**a** hmr-git1Δ::RS-URA3f-loxP-256xlacO-RS ade2-1::(HIS3p-GFP-lacI::ADE2)$_2$ cdc20::MET3p-cdc20::loxP MCD1-TAP::natMX trp1-1::(ADH1p-OsTIR1(codon optimized)::TRP1)$_n$ eco1-3xmAID-5xflag::bleMX ura3Δ::AgTEFp-SpHIS5 bar1Δ can1-100 his3-11,15 leu2-3,112*	MRG7270.1	“”	6B, S5A, S5C, S5D
MRG7300.1	*MAT**a** hmr-git1Δ::RS-URA3f-loxP-256xlacO-RS ade2-1::HIS3p-GFP-lacI-3xmCherry::hphMX::ADE2::HIS3p-GFP-lacI::ADE2 cdc20::MET3p-cdc20::loxP MCD1-*	MRG7269.1	“”	6B

	TAP::natMX trp1-1::(ADH1p-OsTIR1(codon optimized)::TRP1)$_n$ eco1-3xmAID-5xflag::bleMX ura3Δ::AgTEFp-SpHIS5 bar1Δ can1-100 his3-11,15 leu2-3,112			
MRG7302.1	*MAT***a** *hmr-git1Δ::RS-URA3f-loxP-256xlacO-RS ade2-1::HIS3p-GFP-lacI-4xmCherry::kanMX::ADE2::HIS3p-GFP-lacI::ADE2 cdc20::MET3p-cdc20::loxP MCD1-TAP::natMX trp1-1::(ADH1p-OsTIR1(codon optimized)::TRP1)$_n$ eco1-3xmAID-5xflag::bleMX ura3Δ::AgTEFp-SpHIS5 bar1Δ can1-100 his3-11,15 leu2-3,112*	MRG7275.1	“”	6B
MRG7270.1	*MAT***a** *hmr-git1Δ::RS-URA3f-loxP-256xlacO-RS ade2-1::(HIS3p-GFP-lacI::ADE2)$_2$ cdc20::MET3p-cdc20::loxP MCD1-TAP::natMX trp1-1::(ADH1p-OsTIR1(codon optimized)::TRP1)$_n$ ura3Δ::AgTEFp-SpHIS5 bar1Δ can1-100 his3-11,15 leu2-3,112*	MRG6964 X MRG7258.2	“”	6C, S5A, S5D
MRG7269.1	*MAT***a** *hmr-git1Δ::RS-URA3f-loxP-256xlacO-RS ade2-1::HIS3p-GFP-lacI-3xmCherry::hphMX::ADE2::HIS3p-GFP-lacI::ADE2 cdc20::MET3p-cdc20::loxP MCD1-TAP::natMX trp1-1::(ADH1p-OsTIR1(codon optimized)::TRP1)$_n$ ura3Δ::AgTEFp-SpHIS5 bar1Δ can1-100 his3-11,15 leu2-3,112*	MRG6964 X MRG7258.2	“”	6C, S5B
MRG7275.1	*MAT***a** *hmr-git1Δ::RS-URA3f-loxP-256xlacO-RS ade2-1::HIS3p-GFP-lacI-4xmCherry::kanMX::ADE2::HIS3p-GFP-lacI::ADE2 cdc20::MET3p-cdc20::loxP MCD1-TAP::natMX trp1-1::(ADH1p-OsTIR1(codon optimized)::TRP1)$_n$ ura3Δ::AgTEFp-SpHIS5 bar1Δ can1-100 his3-11,15 leu2-3,112*	MRG7240.1 X MRG7258.2	“”	6C
MRG7151	*MAT***a** *hmr-git1Δ::RS-URA3f-lacOPs-RS ade2-1::(HIS3p-GFP-lacI::ADE2)$_2$ cdc20::MET3p-cdc20::loxP leu2-3,112::GAL1p-SIC1(4m)-AID*-9xmyc::LEU2 MCD1-TAP::natMX ura3Δ::AgTEFp-SpHIS5 smc1-D1164E bar1Δ can1-100 his3-11,15 trp1-1*	MRG6792 X MRG7027	“”	6D
MRG7146	*MAT***a** *hmr-git1Δ::RS-URA3f-lacOPs-RS ade2-1::HIS3p-GFP-lacI-3xmCherry::hphMX::ADE2::HIS3p-GFP-lacI::ADE2 cdc20::MET3p-cdc20::loxP leu2-3,112::GAL1p-SIC1(4m)-AID*-9xmyc::LEU2 MCD1-TAP::natMX ura3Δ::AgTEFp-SpHIS5 smc1-D1164E bar1Δ can1-100 his3-11,15 trp1-1*	MRG6887 X MRG7130	“”	6D

MRG7159	*MAT***a** *hmr-git1Δ::RS-URA3f-lacOPs-RS ade2-1::HIS3p-GFP-lacI-4xmCherry::kanMX::ADE2::HIS3p-GFP-lacI::ADE2 cdc20::MET3p-cdc20::loxP leu2-3,112::GAL1p-SIC1(4m)-AID*-9xmyc::LEU2 MCD1-TAP::natMX ura3Δ::AgTEFp-SpHIS5 smc1-D1164E bar1Δ can1-100 his3-11,15 trp1-1*	MRG7146 X MRG7150	“”	6D
MRG7327.1	*MAT***a** *hmr-git1Δ::RS-URA3f-loxP-256xlacO-RS ade2-1::(HIS3p-GFP-lacI::ADE2)$_2$ cdc20::MET3p-cdc20::loxP MCD1-TAP::natMX trp1-1::(ADH1p-OsTIR1(codon optimized)::TRP1)$_n$ wpl1-3xmAID-5xflag::bleMX ura3Δ::AgTEFp-SpHIS5 bar1Δ can1-100 his3-11,15 leu2-3,112*	MRG7270.1	“”	6E, S5A, S5C, S5D
MRG7329.1	*MAT***a** *hmr-git1Δ::RS-URA3f-loxP-256xlacO-RS ade2-1::HIS3p-GFP-lacI-3xmCherry::hphMX::ADE2::HIS3p-GFP-lacI::ADE2 cdc20::MET3p-cdc20::loxP MCD1-TAP::natMX trp1-1::(ADH1p-OsTIR1(codon optimized)::TRP1)$_n$ wpl1-3xmAID-5xflag::bleMX ura3Δ::AgTEFp-SpHIS5 bar1Δ can1-100 his3-11,15 leu2-3,112*	MRG7269.1	“”	6E, S5B
MRG7324.1	*MAT***a** *hmr-git1Δ::RS-URA3f-loxP-256xlacO-RS ade2-1::HIS3p-GFP-lacI-4xmCherry::kanMX::ADE2::HIS3p-GFP-lacI::ADE2 cdc20::MET3p-cdc20::loxP MCD1-TAP::natMX trp1-1::(ADH1p-OsTIR1(codon optimized)::TRP1)$_n$ wpl1-3xmAID-5xflag::bleMX ura3Δ::AgTEFp-SpHIS5 bar1Δ can1-100 his3-11,15 leu2-3,112*	MRG7275.1	“”	6E
MRG7332.1	*MAT***a** *hmr-git1Δ::RS-URA3f-loxP-256xlacO-RS ade2-1::(HIS3p-GFP-lacI::ADE2)$_2$ cdc20::MET3p-cdc20::loxP MCD1-TAP::natMX trp1-1::(ADH1p-OsTIR1(codon optimized)::TRP1)$_n$ wpl1-3xmAID-5xflag::bleMX eco1-3xmAID-5xflag::kanMX ura3Δ::AgTEFp-SpHIS5 bar1Δ can1-100 his3-11,15 leu2-3,112*	MRG7327.1	“”	6F, S5A, S5C, S5D
MRG7356.1	*MAT***a** *hmr-git1Δ::RS-URA3f-loxP-256xlacO-RS ade2-1::HIS3p-GFP-lacI-3xmCherry::hphMX::ADE2::HIS3p-GFP-lacI::ADE2 cdc20::MET3p-cdc20::loxP MCD1-TAP::natMX trp1-1::(ADH1p-OsTIR1(codon optimized)::TRP1)$_n$ wpl1-3xmAID-5xflag::bleMX eco1-3xmAID-5xflag::kanMX ura3Δ::AgTEFp-SpHIS5 bar1Δ can1-100 his3-11,15 leu2-3,112*	MRG7329.1	“”	6F
MRG7353.1	*MAT***a** *hmr-git1Δ::RS-URA3f-loxP-256xlacO-RS*	MRG7337.1	“”	6F

	ade2-1::HIS3p-GFP-lacI-4xmCherry::hphMX::ADE2::HIS3p-GFP-lacI::ADE2 cdc20::MET3p-cdc20::loxP MCD1-TAP::natMX trp1-1::(ADH1p-OsTIR1(codon optimized)::TRP1)$_n$ wpl1-3xmAID-5xflag::bleMX eco1-3xmAID-5xflag::kanMX ura3Δ::AgTEFp-SpHIS5 bar1Δ can1-100 his3-11,15 leu2-3,112			
MSB203	*MAT***a** *hmr-git1Δ::RS-URA3f-loxP-256xlacO-RS ade2-1::(HIS3p-GFP-lacI::ADE2)$_2$ cdc20::MET3p-cdc20::loxP MCD1-TAP::natMX leu2-3,112:(GAL1p-RecR::LEU2)$_2$ trp1-1::(ADH1p-OsTIR1(codon optimized)::TRP1)$_n$ ura3Δ::AgTEFp-SpHIS5 bar1Δ can1-100 his3-11,15*	MRG7270.1	“”	6G
MSB204	*MAT***a** *hmr-git1Δ::RS-URA3f-loxP-256xlacO-RS ade2-1::(HIS3p-GFP-lacI::ADE2)$_2$ cdc20::MET3p-cdc20::loxP MCD1-TAP::natMX leu2-3,112:(GAL1p-RecR::LEU2)$_2$ trp1-1::(ADH1p-OsTIR1(codon optimized)::TRP1)$_n$ eco1-3xmAID-5xflag::bleMX ura3Δ::AgTEFp-SpHIS5 bar1Δ can1-100 his3-11,15*	MRG7301.1	“”	6G
MSB205	*MAT***a** *hmr-git1Δ::RS-URA3f-loxP-256xlacO-RS ade2-1::(HIS3p-GFP-lacI::ADE2)$_2$ cdc20::MET3p-cdc20::loxP MCD1-TAP::natMX leu2-3,112:(GAL1p-RecR::LEU2)$_2$ trp1-1::(ADH1p-OsTIR1(codon optimized)::TRP1)$_n$ wpl1-3xmAID-5xflag::bleMX ura3Δ::AgTEFp-SpHIS5 bar1Δ can1-100 his3-11,15*	MRG7327.1	“”	6G
MSB206	*MAT***a** *hmr-git1Δ::RS-URA3f-loxP-256xlacO-RS ade2-1::(HIS3p-GFP-lacI::ADE2)$_2$ cdc20::MET3p-cdc20::loxP MCD1-TAP::natMX leu2-3,112:(GAL1p-RecR::LEU2)$_2$ trp1-1::(ADH1p-OsTIR1(codon optimized)::TRP1)$_n$ wpl1-3xmAID-5xflag::bleMX eco1-3xmAID-5xflag::kanMX ura3Δ::AgTEFp-SpHIS5 bar1Δ can1-100 his3-11,15*	MRG7332.1	“”	6G
MRG7372	*MAT***a** *hmr-git1Δ::RS ade2-1::(HIS3p-GFP-lacI::ADE2)$_2$ leu2-3,112::(GAL1p-RecR::LEU2)$_2$ cdc20::MET3p-cdc20::loxP can1-100 his3-11,15 trp1-1 ura3-1*	MSB35.2	“”	S1B
MRG7373	*MAT***a** *hmr-git1Δ::RS ade2-1::HIS3p-GFP-lacI-3xmCherry::hphMX::ADE2::HIS3p-GFP-lacI::ADE2 leu2-3,112::(GAL1p-RecR::LEU2)$_2$ cdc20::MET3p-cdc20::loxP can1-100 his3-11,15 trp1-1 ura3-1*	MSB167	“”	S1B
MRG7374	*MAT***a** *hmr-git1Δ::RS ade2-1::HIS3p-GFP-lacI-4xmCherry::kanMX::ADE2::HIS3p-GFP-*	MRG7060	“”	S1B

	lacI::ADE2 leu2-3,112::(GAL1p-RecR::LEU2)$_2$ cdc20::MET3p-cdc20::loxP MCD1-TAP::natMX ura3Δ::AgTEFp-SpHIS5 can1-100 his3-11,15 trp1-1			
MRG7320	*MAT***a** *hmr-git1Δ::RS-URA3f-loxP-256xlacO-RS ade2-1::HIS3p-GFP-lacI-3xyeGFP(A206R)::kanMX::ADE2::HIS3p-GFP-lacI::ADE2 leu2-3,112::(GAL1p-RecR::LEU2)$_2$ cdc20::MET3p-cdc20::loxP MCD1-TAP::natMX ura3Δ::AgTEFp-SpHIS5 can1-100 his3-11,15 trp1-1*	MSB165.1	“”	S3
MRG7312	*MAT***a** *hmr-git1D::RS-URA3f-lacOPs-RS ade2-1::(HIS3p-GFP-lacI::ADE2)$_2$ cdc20::MET3p-cdc20::loxP ho::GAL1p-mcd1(R180D,R268D)-TAP::natMX::ho mcd1-3xmAID-5xflag::bleMX ura3Δ::AgTEFp-SpHIS5 bar1Δ can1-100 his3-11,15 trp1-1 leu2-3,112 trp1-1*	MRG6989	“”	S5A
MRG7355.1	*MAT***a** *hmr-git1Δ::RS-URA3f-loxP-256xlacO-RS ade2-1::(HIS3p-GFP-lacI::ADE2)$_2$ cdc20::MET3p-cdc20::loxP MCD1-TAP::natMX trp1-1::(ADH1p-OsTIR1(codon optimized)::TRP1)$_n$ wpl1Δ::kanMX eco1-3xmAID-5xflag::bleMX ura3Δ::AgTEFp-SpHIS5 bar1Δ can1-100 his3-11,15 leu2-3,112*	MRG7301.1	“”	S5A
MRG7329 (isolate #1)	*MAT***a** *hmr-git1Δ::RS-URA3f-loxP-256xlacO-RS ade2-1::HIS3p-GFP-lacI-3xmCherry::hphMX::ADE2::HIS3p-GFP-lacI::ADE2 cdc20::MET3p-cdc20::loxP MCD1-TAP::natMX trp1-1::(ADH1p-OsTIR1(codon optimized)::TRP1)$_n$ wpl1-3xmAID-5xflag::bleMX ura3Δ::AgTEFp-SpHIS5 bar1Δ can1-100 his3-11,15 leu2-3,112*	MRG7269.1		S5B
MRG6830.1	*MAT***a** *hmr-git1Δ::RS-URA3f-loxP-256xlacO-RS ade2-1::HIS3p-GFP-lacI-3xmCherry::hphMX::ADE2::HIS3p-GFP-lacI::ADE2 leu2-3,112::(GAL1p-RecR::LEU2)$_2$ cdc20::MET3p-cdc20::loxP MCD1-TAP::natMX ura3Δ::AgTEFp-SpHIS5 wpl1Δ::TRP1 can1-100 his3-11,15 trp1-1*	MSB165.1	“”	S5B
MRG7235.1	*MAT***a** *hmr-git1Δ::RS-URA3f-loxP-256xlacO-RS ade2-1::(HIS3p-GFP-lacI::ADE2)$_2$ leu2-3,112::GAL1p-SIC1(4m)-AID*-9xmyc::LEU2 cdc20::MET3p-cdc20::loxP MCD1-TAP::natMX wpl1Δ::TRP1 ura3Δ::AgTEFp-SpHIS5 bar1Δ can1-100 his3-11,15 trp1-1*	MRG7027	“”	S6A, S6B
MRG7232.1	*MAT***a** *hmr-git1Δ::RS-URA3f-loxP-256xlacO-RS ade2-1::HIS3p-GFP-lacI-3xmCherry::hphMX::ADE2::HIS3p-GFP-*	MRG7026	“”	S6A

	lacI::ADE2 leu2-3,112::GAL1p-SIC1(4m)-AID-9xmyc::LEU2 cdc20::MET3p-cdc20::loxP MCD1-TAP::natMX wpl1Δ::TRP1 ura3Δ::AgTEFp-SpHIS5 bar1Δ can1-100 his3-11,15 trp1-1*			
MRG7238.1	*MAT***a** *hmr-git1Δ::RS-URA3f-loxP-256xlacO-RS ade2-1::HIS3p-GFP-lacI-4xmCherry::kanMX::ADE2::HIS3p-GFP-lacI::ADE2 leu2-3,112::GAL1p-SIC1(4m)-AID*-9xmyc::LEU2 cdc20::MET3p-cdc20::loxP MCD1-TAP::natMX wpl1Δ::TRP1 ura3Δ::AgTEFp-SpHIS5 bar1Δ can1-100 his3-11,15 trp1-1*	MRG7059	“”	S6A
MRG7115	*MAT***a** *hmr-git1Δ::RS-URA3f-loxP-256xlacO-RS ade2-1::HIS3p-GFP-lacI-3xmCherry::hphMX::ADE2 leu2-3,112::GAL1p-SIC1(4m)-AID*-9xmyc::LEU2 cdc20::MET3p-cdc20::loxP MCD1-TAP::natMX ura3Δ::AgTEFp-SpHIS5 bar1Δ can1-100 his3-11,15 trp1-1*	MRG6919 x MRG7041	“”	S7
MRG7122	*MAT***a** *hmr-git1Δ::RS-URA3f-loxP-256xlacO-RS ade2-1::HIS3p-GFP-lacI-4xmCherry::kanMX::ADE2 leu2-3,112::GAL1p-SIC1(4m)-AID*-9xmyc::LEU2 cdc20::MET3p-cdc20::loxP MCD1-TAP::natMX ura3Δ::AgTEFp-SpHIS5 bar1Δ can1-100 his3-11,15 trp1-1*	MRG7102 x MRG7041	“”	S7

Table S2 – Oligonucleotides

Name	Sequence (5'-3')	Use
5'lacO F	GCGTTACCCAACTTAATCGC	ChIP-qPCR
5'lacO R	CACAGCTTGTCTGTAAGCG	""
549.7 S	TGAAGATGACATTGCTCCTTT	""
549.7 AS	TGGATAATGGATCTGAAACCG	""
534 S	ACAAGCATCATTCATAGCCT	""
534 AS	ATCGTGGCTAGGACATTTTG	""
URA3 F	AGAATTGTCATGCAAGGGCTC	RT-qPCR
URA3 R	TCAAATATGCTTCCCAGCCT	""
5' ACT1 (F)	CGTTACCCAATTGAACACGGT	""
3' ACT1 (R)	AAGGACAAAACGGCTTGGAT	""
1xmCherry F	TAATGCAGCTGGGATCCTGTACTCCACCAAAGAAGAAGAGAAA GGTTGCCCTCGACGGAGCTGGTATGGTTTCTAAG	Strain construction
2xmCherry F	TAATGCAGCTGGGATCCTGTACTCCACCAAAGAAGAAGAGAAA GGTTGCCCTCGACGGTGCTGGAATGGTGTCCAAA	""
3xmCherry F	TAATGCAGCTGGGATCCTGTACTCCACCAAAGAAGAAGAGAAA GGTTGCCCGTACGCTGCAGGTCGAC	""
4xmCherry F	AAAGAGCAGAAGGACGACATTCCACAGGTGGCATGGACGAGTT ATACAAGCTCGACGGAGCTGGTATGGTTTCTAAG	""
mCherry R	GAATTCCTGCAGCCCGGGGGATCCACTAGTTCTAGAGCGGCCGC TCTAGATTAAAGCCTTCGAGCGTCC	""
3xmAID WPL1 F	TAGCGTTAAATTACCTAAAATCAATATACACGAGTGAAAGAATT ACAATAGCTGGTGCAGGTGCCGGTAAAGAAAAGAGT	""
3xmAID WPL1 R	GTTGCCAGCAGGGTGAAGATGAAGCCAGGCTATGTTCAATGTAT GCTTTCTTTAGCATAGGCCACTAGTGGATCTGATAT	""
3xmAID ECO1 F	CAACGGCATTATGCATAAATCAGGCAAGTTACTATTGCCGGTAT ACATAGCTGGTGCAGGTGCCGGTAAAGAAAAGAGT	""
3xmAID ECO1 R	TTTATGCCATTTTTCCAGTGTCCCTTCTCGCTGTCTTTTCGAAAGA GTCAGCATAGGCCACTAGTGGATCTGATAT	""
SIC1 AID*-9xmyc F	GATGAAGAAAAGAGAAGATTCAAGCCAAAGGCATTGTTTCAAT CTAGGGATCAAGAGCATCGTACGCTGCAGGTCGAC	Plasmid construction
M13-T7-AID*-9xmyc R	TGTAAAACGACGGCCAGTGAGCGCGCGTAATACGACTCACTATA GGGGCGCCTTTTTAGCTAGTG	""
URA3-N site a F	TAAGGAACGTGCTGCTACTC	ChIP-qPCR
URA3-N site a R	TTGGCGGATAATGCCTTTAGCG	""
URA3 site b F	GCTCAAAGAGACATGGGTGAA	""
URA3 site b R	GCCGCATCTTCTCAAATATGC	""
ChrIII site c F	CAAAGTTGTGCTTTGGAT	""
ChrIII site c R	ACTTTCTAAGACGCTAGGA	""
ChrIII site d F	GTAATGGAGGCCTCGGATAATG	""
ChrIII site d R	ACGAGTCAAGGCGGTAAT	""
ChrIII site e F	CTCGTTATGCCCGTCATC	""
ChrIII site e R	AGTCTAGCAAGGATTCTGAC	""
ChrIII site f F	CCCTTACCTAACTGGTCTCTC	""
ChrIII site f R	CAGTGGGCTCTTGTACC	""
ChrIII site g F	CACTAGATTGAGACCAGCC	""
ChrIII site g R	CCAGAAGGATAGCCTAGAAGA	""